AD-A179 699 FUNDAMENTAL STUDIES OF THE MECHANICAL BEHAVIOR OF MICROELECTRONIC THIN FI.. (U) STANFORD UNIV CA DEPT OF MATERIALS SCIENCE AND ENGINEERING W D NIX MAR 87 1/1

UNCLASSIFIED AFOSR-TR-87-0411 AFOSR-86-0051 F/G 9/3 NL

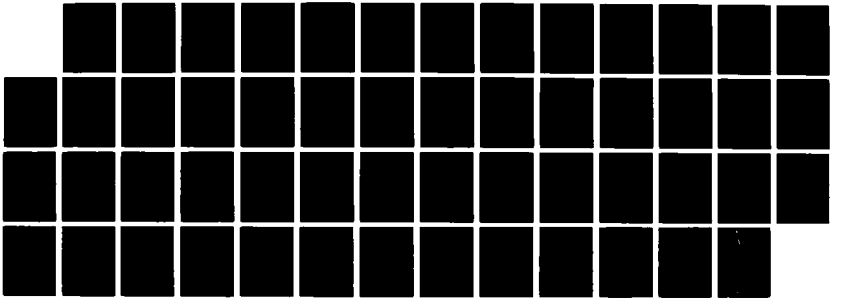

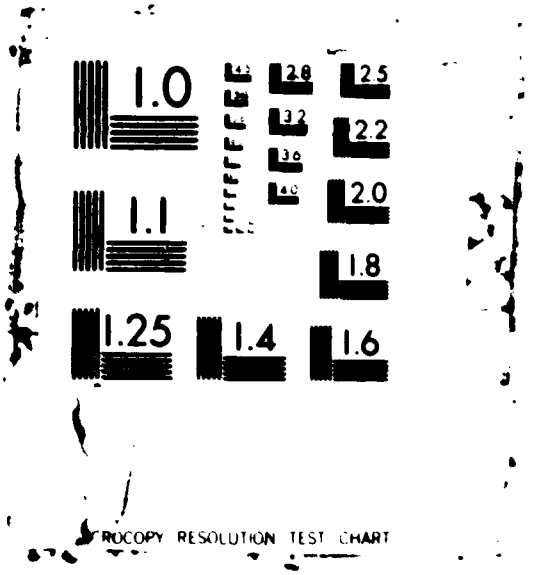
1.0
1.1
1.25
1.4
1.6
2.8
3.2
3.6
4.0
2.5
2.2
2.0
1.8
ROCOPY RESOLUTION TEST CHART

SECU

DTIC FILE COPY

AD-A179 699

RT DOCUMENTATION PAGE

1a. R	1b. RESTRICTIVE MARKINGS
2a. SECURITY CLASSIFICATION AUTHORITY	3. DISTRIBUTION/AVAILABILITY OF REPORT Unlimited
2b. DECLASSIFICATION/DOWNGRADING SCHEDULE	
4. PERFORMING ORGANIZATION REPORT NUMBER(S)	5. MONITORING ORGANIZATION REPORT NUMBER(S) AFOSR-TR- 87-0411
6a. NAME OF PERFORMING ORGANIZATION Stanford Univ.	6b. OFFICE SYMBOL (If applicable)
6c. ADDRESS (City, State and ZIP Code) Stanford University Stanford CA 94305	7a. NAME OF MONITORING ORGANIZATION AFOSR/NE
	7b. ADDRESS (City, State and ZIP Code) BLDG 410 Bolling AFB DC 20332
8a. NAME OF FUNDING/SPONSORING ORGANIZATION AFOSR	8b. OFFICE SYMBOL (If applicable) NE
	9. PROCUREMENT INSTRUMENT IDENTIFICATION NUMBER AFOSR 86-0051
8c. ADDRESS (City, State and ZIP Code) same as 7b	10. SOURCE OF FUNDING NOS.

PROGRAM ELEMENT NO.	PROJECT NO.	TASK NO.	WORK UNIT NO.
61102f	2306	A1	

11. TITLE (Include Security Classification)
Fundamental Studies of the Mechanical Behavior of Microelectronic Thin Film Materials

12. PERSONAL AUTHOR(S)
Nix

13a. TYPE OF REPORT	13b. TIME COVERED	14. DATE OF REPORT (Yr., Mo., Day)	15. PAGE COUNT
Annual	FROM 11-1-85 TO 10-31-86	MARCH 87	

16. SUPPLEMENTARY NOTATION

17. COSATI CODES			18. SUBJECT TERMS (Continue on reverse if necessary and identify by block number)
FIELD	GROUP	SUB. GR.	

19. ABSTRACT (Continue on reverse if necessary and identify by block number)

20. DISTRIBUTION/AVAILABILITY OF ABSTRACT
UNCLASSIFIED/UNLIMITED ☒ SAME AS RPT ☐ DTIC USERS ☐

21. ABSTRACT SECURITY CLASSIFICATION
UUUU

22a. NAME OF RESPONSIBLE INDIVIDUAL	22b. TELEPHONE NUMBER (Include Area Code)	22c. OFFICE SYMBOL
Dr. Rosenstein	767-4931	NE

DD FORM 1473, 83 APR EDITION OF 1 JAN 73 IS OBSOLETE.

SECURITY CLASSIFICATION OF THIS PAGE

Interim Scientific Report
(For the Period 1 November 1985 to 31 October 1986)
AFOSR GRANT NO. 86-0051

FUNDAMENTAL STUDIES OF THE MECHANICAL BEHAVIOR OF MICROELECTRONIC THIN FILM MATERIALS

Submitted to:

Department of the Air Force
Directorate of Electronic and Material Sciences
Air Force Office of Scientific Research
Bolling Air Force Base, Building 410
Washington, D.C. 20332

Attention: Dr. Alan H. Rosenstein

Submitted by:

Professor William D. NIx, Principal Investigator
Department of Materials Science and Engineering
Stanford University, Stanford California 94305

March 1987

This research was supported by the Air Force of Scientific Research (AFOSC) under Grant No. AFOSR-86-0051. Approved for public release; distribution unlimited.

Table of Contents

I. Summary

A fundamental program of research on the mechanical properties of microelectronic thin film materials has been initiated at Stanford University. The work is being supported under AFOSR Grant No. 86-0051. In this Interim Scientific Report, some of the progress made during the first year of the program is reviewed. We have made very rapid progress, especially in the development of new experimental techniques for measuring mechanical properties. The work has already led to several publications and to an equal number of invited oral presentations, both of which are listed at the end of this report.

The primary motivation of this work is to understand the mechanical properties of microelectronic thin film materials. Although these materials are not structural materials as such, they are, nevertheless, expected to withstand very high stresses, both during manufacturing and in service. As a consequence, the mechanical properties of these materials are almost as important as their electronic properties for successful device applications. Because these materials often exist only as thin films bonded to substrates, it is necessary to study their mechanical properties in that state. Much of the work of this research program deals with the development of techniques and methods for studying these properties. Also, these techniques are being used to measure various thin film mechanical properties and efforts are being made to understand these properties in fundamental terms.

Sub-micron indentation techniques for measuring the hardness and elastic properties of thin film materials have been developed. These measurement are made with the Nanoindenter. The key feature of the Nanoindenter is the displacement resolution, which is about 0.2 nm (2 Angstroms!). With this resolution it is possible to indent films as thin as 100 nm and obtain elastic and plastic properties from the indentation data. We have also developed a technique for determining the elastic properties of a thin film on a substrate. Because the substrate deforms elastically when the thin film is indented it is necessary to remove the effects of the substrate from the data to obtain the elastic properties of the film.

We have also developed a wafer curvature technique for measuring the stresses in

thin films on substrates and for studying the mechanical properties of thin films, especially at elevated temperatures. This work has been led by Professor Paul Flinn, a Consulting Professor with Intel Corporation. The design principles that have been used to build the wafer curvature machine in our laboratory are described below. Also, the resolution of the system for detecting stresses and for measuring mechanical properties of thin films on substrates is described.

The plastic properties of two candidate interconnect metals, aluminum and tungsten, have been studied using both the Nanoindenter and the Wafer Curvature Machine. We find the strength of thin aluminum films to increase with decreasing thickness. For the case of tungsten we find the strength to decrease with decreasing thickness. We believe this unusual effect is caused by the elastic interactions of dislocations within the films with the phases in contact with the film. For tungsten, the substrate and film oxide are both elastically more compliant than the film itself and this causes dislocations to be attracted to these phases and to move more easily in the film. The substrate and film oxide are stiffer than aluminum so dislocations are repelled in that case and strengthening effects are observed.

The method of images has been used to study the behavior of dislocations in thin films on substrates. Some of the problems we have solved and some of the results we have obtained are reported here. We believe the theoretical methods we have developed can be used to understand dislocation behavior in thin films and the corresponding mechanical properties of these films.

The problem of metal cracking in interconnects is described and a technique for studying this phenomenon is proposed. Some estimates of the stresses expected in metal lines in test structures are made and the wafer curvature effects associated with these stresses are computed. It is shown that time dependent metal cracking can be studied by measuring the changes of curvature associated with the cracking process.

II. Research Report

A. Determination of Mechanical Properties of Thin Films from Indentation Experiments

(M. F. Doerner and W. D. Nix)

1. Introduction

The need for techniques to study the mechanical properties of thin films has recently rekindled an interest in microhardness and sub-micron indentation devices. Because thin film measurements require the use of very small indentations, it has been recognized that depth-sensing instruments are needed to provide the necessary resolution and repeatability in the measurement of hardness. Since conventional microhardness testers require direct imaging of the indentations to obtain hardness, large errors are introduced due to measurement of the diagonal lengths, especially when the indentations are small. In addition, the depth-sensing instrument offers other advantages such as the ability to obtain information about the elastic and time-dependent plastic properties of the sample.

Although indentation hardness testing has been in wide-spread use for almost a century, high resolution depth-sensing instruments have only recently become common. Most of the instruments in use have been built by individual investigators to meet their specific research requirements [1-4]. Standard methods for interpreting the load-displacement curves obtained from these instruments, however, have yet to be established. Since depth-sensing instruments record the total penetration of the indenter into the sample, a method for determining the elastic and plastic contributions to the displacement is required. A technique for subtracting the elastic displacement from the total displacement to obtain the hardness is proposed. Also, a method for relating the elastic displacements to Young's modulus of the sample is described. These methods have been applied to data obtained using a commercially available instrument, the Nanoindenter from Nano Instruments Inc.

2. The Nanoindenter

Athough the data analysis methods descibed here are applicable to any depth-sensing indentation instrument, some of the details of the discussion are specific to the Nanoindenter. For this reason, a brief description of the Nanoindenter operation will be given here.

A schematic diagram of the indenting mechanism is given in Fig. A1. The indenter is a triangular pyramid-shaped diamond with the same area to depth ratio as the traditional Vickers pyramid. The position of the indenter is determined by a capacitance displacement gage. A coil and magnet assembly located at the top of the loading column is used to drive the indenter toward the sample. The force imposed on the column is controlled by varying the current in the coil. The loading column is suspended by flexible springs and the motion is damped by air flow around the center plate of the capacitor, which is attached to the loading column. The capacitance displacement gage permits one to detect displacement changes of 0.2-0.3 nm. The force resolution of the system is about 0.5 μN. Tester operation, including indentation rate control and data recording, is computer controlled.

A typical test involves moving the indenter to the surface of the material and measuring the forces and displacements associated with the indentation process. The surface is located for each indentation by lowering the indenter at a constant rate against the suspending springs and detecting a change in velocity on contact with the surface. In the testing mode, the load is incremented in order to maintain a constant velocity, although other schemes such as a constant strain rate can be implemented. A typical testing rate is about 3 nm per second. A typical loading curve is shown in Fig. A2. The depth plotted represents the total displacement of the indenter relative to the initial position of the surface. It is composed of both elastic and plastic displacements.

THE NANOINDENTER

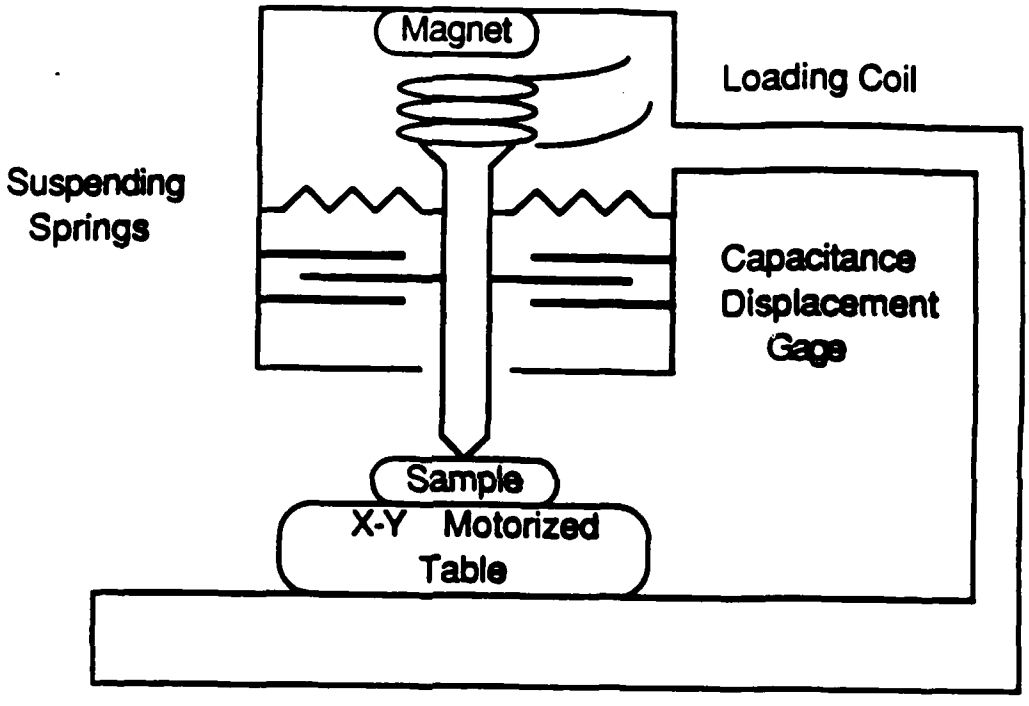

Fig. A1 Schematic diagram of the indenting mechanism of the Nanoindenter.

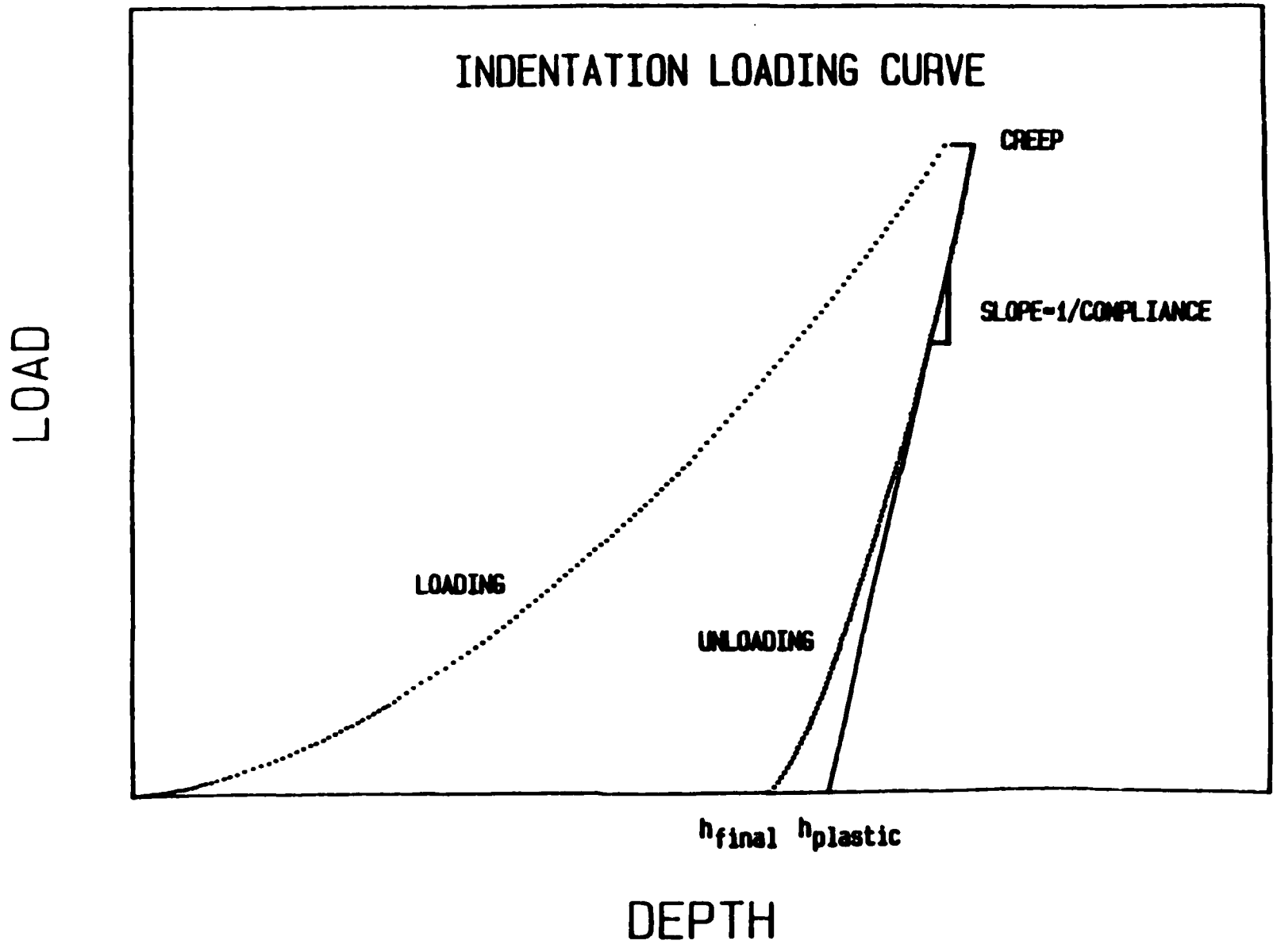

Fig. A2 Typical load-displacement curve obtained using the Nanoindenter showing the difference between the plastic and final depths.

3. Hardness Measurements

Hardness is the equivalent of the average pressure under the indenter, calculated as the applied load divided by the projected area of contact between the indenter and the sample. In a conventional microhardness test, the area of contact is determined by imaging of the indentation after the load is removed and measuring the diagonal lengths. At least for metals, there is little change in the diameter of the indentation on unloading [5] so that the conventional hardness test is essentially a test of hardness under load, although it is subject to some error due to the varying elastic contraction of the diagonal.

Hardness data can be obtained from a depth-sensing instrument without imaging the indentations. This feature provides greatly improved repeatability and time savings over conventional microhardness techniques. However, since the depth measured during the indentation includes both plastic and elastic displacements, the elastic contribution must be subtracted from the data to obtain hardness.

4. Indenter Shape Calibration

Knowledge of the exact shape of the pyramidal diamond indenter is critical to the determination of both plastic and elastic properties. Since the indenter is quite blunt, direct imaging of indentations of small size in the SEM is difficult. Therefore, the method of Pethica et al.[1] was adopted for indenter shape calibration. This method consists of making 2-stage carbon replicas of indentations in a soft material and imaging them in the TEM

The results of the indenter shape calibration are shown in Fig. A3. The importance of accurate indenter shape calibration is clearly demonstrated in the hardness data for <111> silicon shown in Fig. A4. These data were obtained from individual indentations, with a 10 second hold at maximum load. Use of the ideal geometry results in a large overestimate of the hardness at small depths since the indenter tip is considerably more blunt than the ideal pyramid. With correction for the indenter geometry, the hardness is

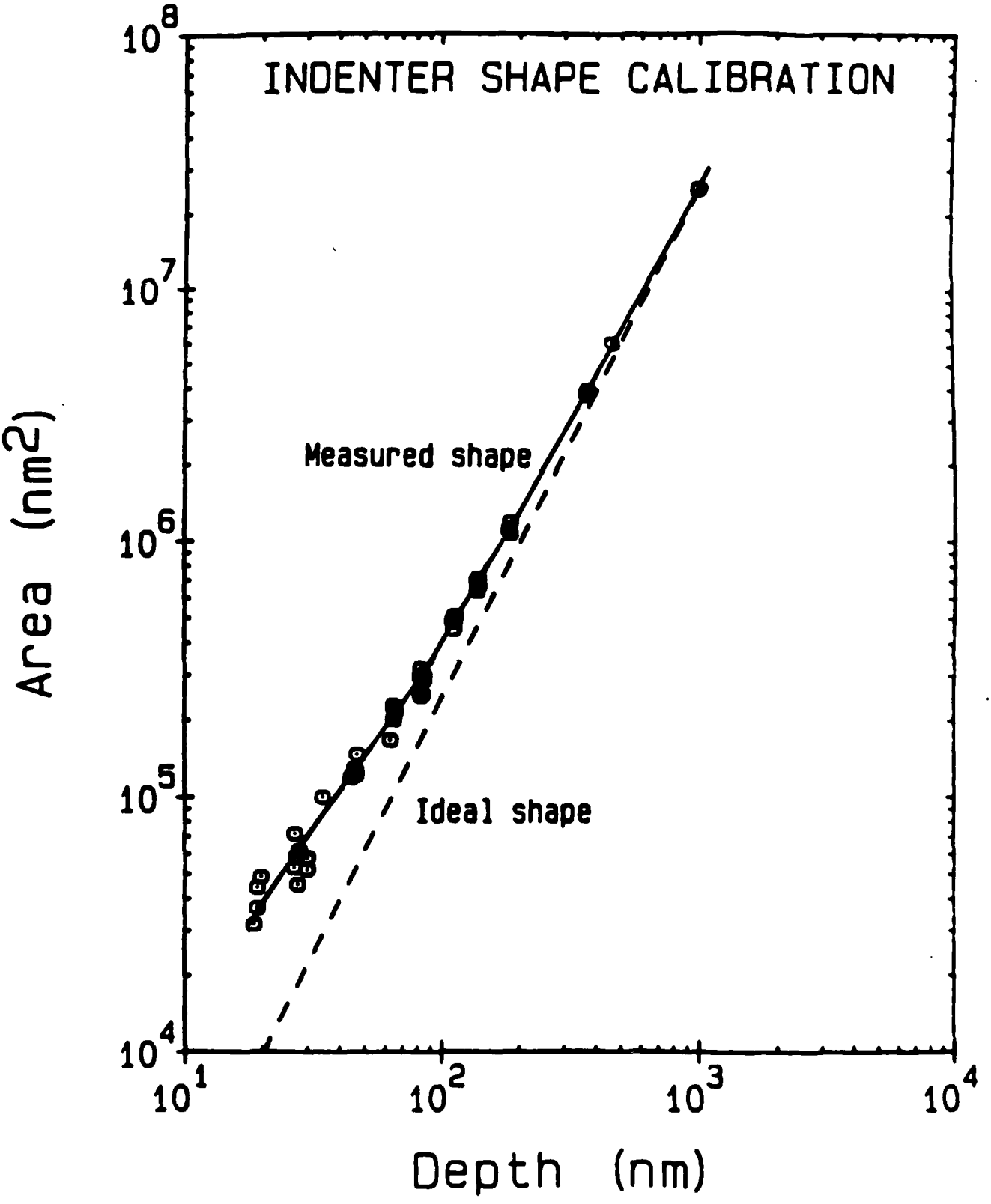

Fig. A3 Shape of the diamond indenter at the tip as determined by the TEM replica technique.

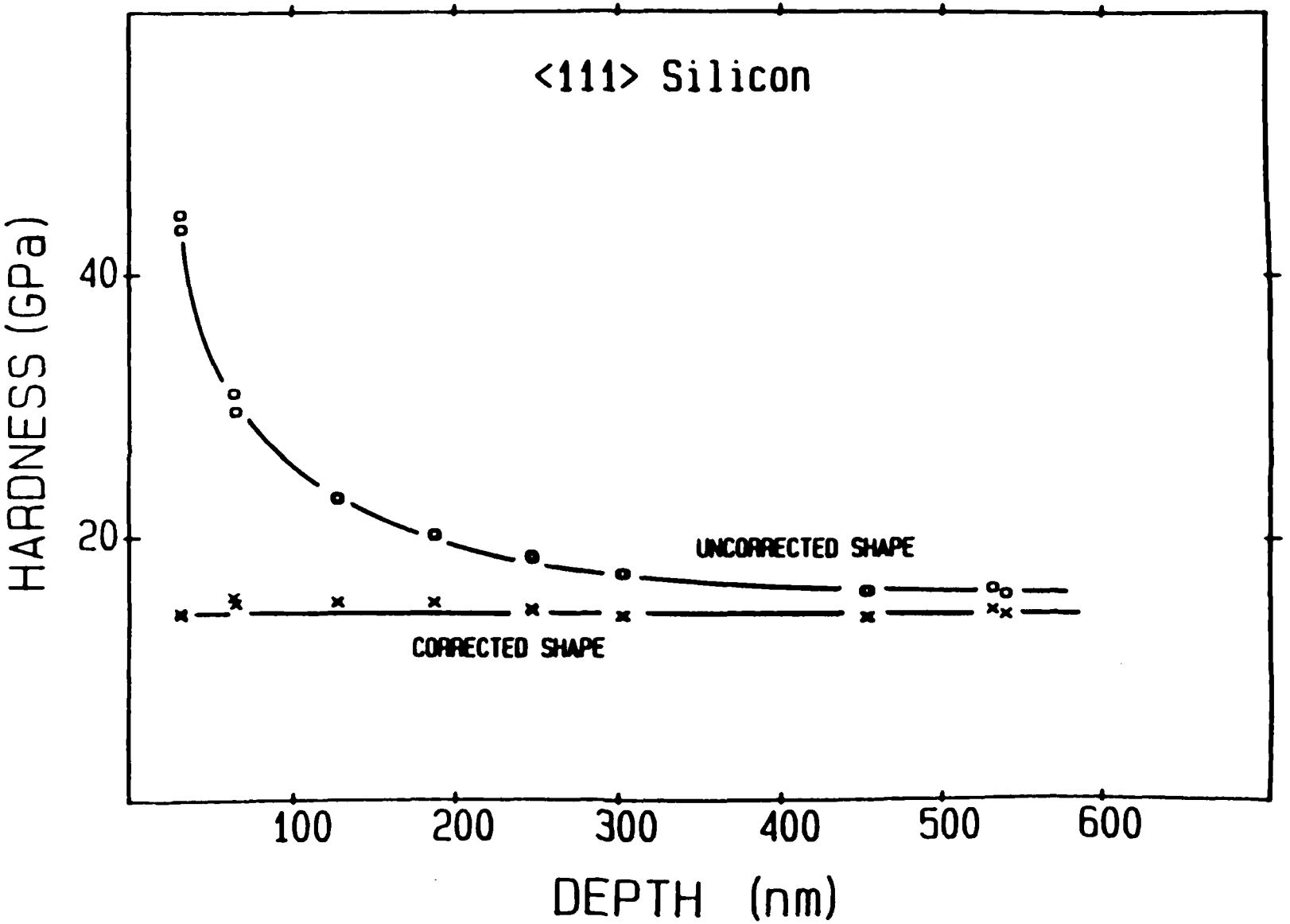

Fig. A4. Hardness as a function of indentation depth for mechanically polished silicon illustrating the importance of accurately determining the shape of the tip of the indenter.

seen to be independent of the depth of indentation.

5. Elastic Properties

The slope of the unloading curve can be used as a measure of the elastic properties of the sample. If the area in contact remains constant during initial unloading, the elastic behavior may be modeled as that of a blunt punch indenting an elastic solid. Young's modulus can then be calculated, provided Poisson's ratio is known. However, it is not necessary to know the value of Poisson's ratio with great precision to obtain a good value of Young's modulus.

Comparison of the predicted and measured elastic properties of various materials is given in Fig. A5. In the case of single crystals, Young's modulus in the indentation direction is used for comparison. Since for cubic crystals, Poisson's ratio is constant in the {111} and {100} planes, and this value was used. Agreement of the data with the predictions is relatively good. The measured slopes generally indicate values for Young's modulus which are higher than actual values. Since tungsten, silicon and SiO_2 all have high ratios of hardness to elastic modulus, large compressive elastic strains are obtained under the indenter. These may lead to measurements in a nonlinear elastic regime. For example, using the third order elastic constants for germanium [6], one can show that an estimated hydrostatic pressure of 10 GPa would reduce the parameter $(1-\nu^2)/E$ by 23% and 11% for the <111> and <100> directions, respectively. The agreement of the data with known values is encouraging, however, and lends credence to the method for removal of the elastic displacements in the calculation of hardness.

6. Summary

Depth-sensing indentation instruments provide a means for studying the plastic and elastic properties of thin films. The elastic displacements can be subtracted from the load-displacement data to calculate hardness. Young's modulus can be calculated from the slope of the linear portion of the unloading curve. In addition, the influence of the elastic

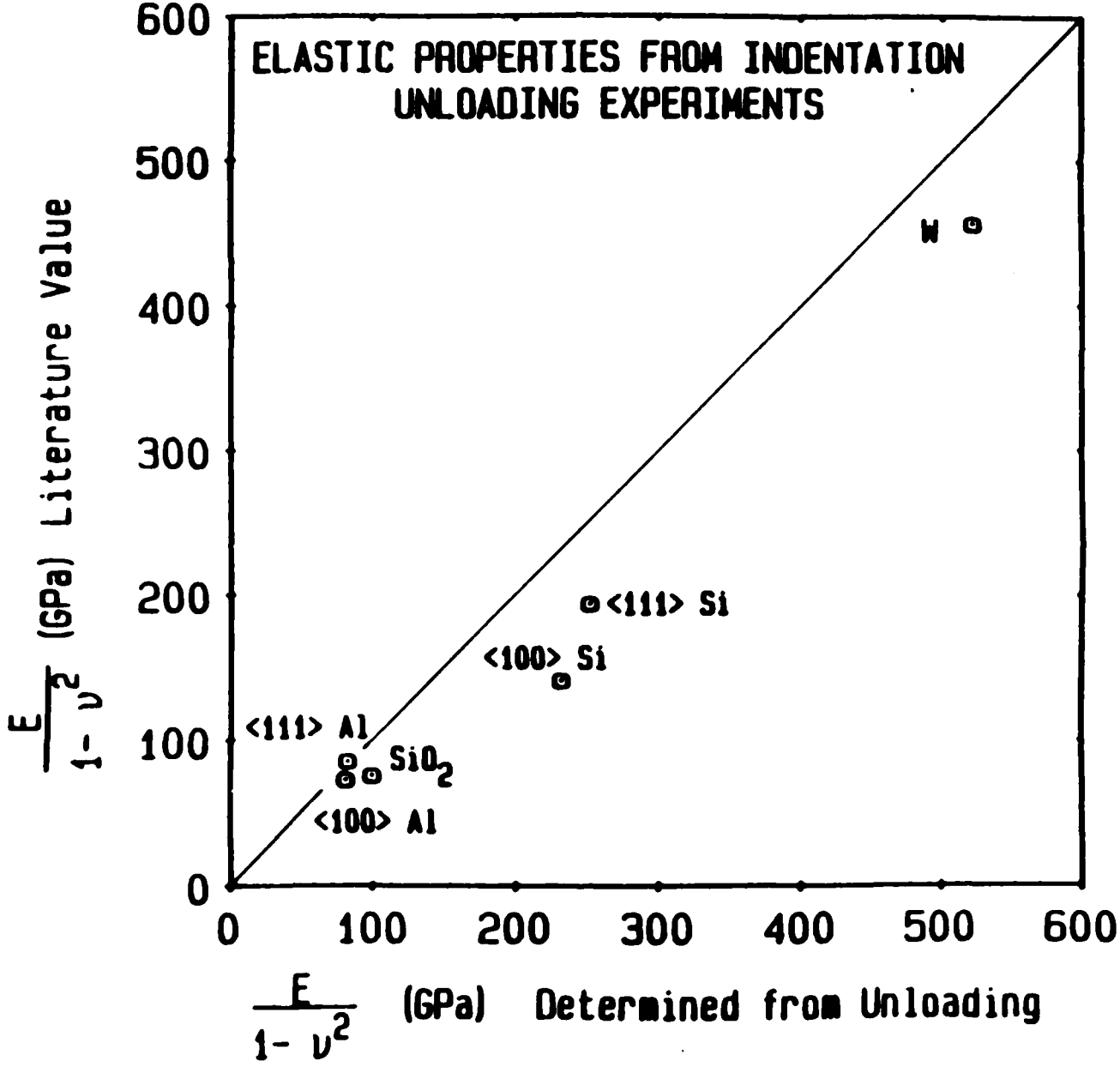

Fig. A5 Comparison of measured elastic properties of various materials with the literature values. The maesured values were obtained from the unloading slopes of indentation curves.

properties of the substrate can be observed in the testing of thin films.

Hardness can be calculated from data along the loading curve, allowing the depth dependence of the hardness to be obtained from one indentation. The effect of strain rate on the measured hardness obtained in this way can be significant.

References

1. J. Pethica, R. Hutchings and W. C. Oliver, Phil. Mag. A, 48, 593 (1983)
2. J. L. Loubet, J. M. Georges, J. M. Marchesini and G. Meille, J. Tribology, 106, 43 (1984)
3. P. E. Wierenga and A. J. J. Frenken, J. Appl. Phys., 55, 4244 (1984)
4. D. Newey, M. A. Wilkins and H. M. Pollock, J. Phys. E: Sci. Instrum., 15, 119 (1982)
5. N. A. Stilwell and D. Tabor, Proc. Phys. Soc., 78, 169 (1961)
6. E. H. Bogardus, J. Appl. Phys., 36, 2504 (1965)

B. Wafer Curvature Techniques for the Study of Mechanical Properties of Thin Films on Substrates

(P.A. Flinn, J.F. Turlo and W.D. Nix)

Mechanical stress in interconnection structures has long been a problem in VLSI devices; continued scaling and the introduction of new materials and processes is increasing the severity of the problem. Several effects contribute to the stresses. The various metallic and dielectric materials used have coefficients of thermal expansion which differ from that of the silicon substrate, so that temperature changes, both during processing and in service, result in stress. In addition, many deposition processes, particularly low temperature processes, which are increasingly popular, result in films with large intrinsic stresses, that is, stress in addition to that which can be accounted for by differences in thermal expansion. Finally, solid state reactions may occur during processing. These reactions normally involve a volume change and an associated stress change.

The stresses which arise from these various causes are often quite large and may exceed the strength of the film, resulting in cracking; or an interface may fail, resulting in delamination. The problems become evident during process development and make an otherwise attractive process non-viable. A problem may appear in production and cause a yield loss or, most serious of all, it may result in delayed failure and thus be a reliability problem. Some examples of the last case are passivation cracks causing delayed failure due to corrosion or metal cracks causing early failure by electromigration. A thorough quantitative understanding of mechanical stress in interconnection materials is of growing importance for the development of new interconnection structures and processes.

The conventional methods of investigating stress in bulk materials have very limited application to interconnection films. Standard testing machines require bulk samples that are normally quite large. Most commonly used dielectrics are made by vapor deposition and are available only as thin films. Metals are, of course, available in bulk but, the structure and properties of metal in the form of a deposited thin film are quite different from those of material of the same chemical composition in bulk form. In

addition, the behavior of a thin film atatched to a substrate may be significantly different from the isolated film. In general, therefore, for either experimental or theoretical investigation, it is necessary to study the film-substrate combination as prepared by the process of interest.

Most methods for determining the stress in a film are based on measurement of the curvature of a uniformly coated wafer and use of the equation,

$$\sigma_f = [E_s t_s^2] / [6(1-\upsilon_s)t_f R].$$

Note that it is only necessary to know the thickness of the film and the substrate, and the elastic properties of the substrate. It is not necessary to know the elastic properties of the film; as long as it is of uniform and known thickness, it may have any composition and microstructure and the stress can still be obtained. Many methods have been used for the curvature measurement, X-ray as well as various optical techniques, but a laser based optical lever technique provides the best combination of accuracy, convenience and speed for most applications.

The basic principle of the technique is quite simple: a laser beam is reflected from the surface of the wafer, and the displacement of the reflected beam is determined as the wafer is scanned. The change in displacement of the reflected beam is proportional to the change in the angle between the incident laser beam and the wafer surface; it is, therefore, a derivative measuring device. For a perfectly flat wafer, the position of the reflected beam would be constant. If the wafer has constant curvature, the angle changes linearly with the relative motion of the wafer and the incident laser beam; consequently, the displacement varies at a rate proportional to the inverse radius of curvature. A plot of beam displacement as a function of scan distance is then a straight line with a slope proportional to the inverse radius of curvature.

The required relative motion of the laser beam and the sample can be accomplished in any one of several ways. The early systems used a fixed laser beam and moved the sample; this is satisfactory for measurements at room temperture, but is awkward for

elevated temperatures. An alternative is the use of a stationary sample (which can be in a furnace) and motion of a combined laser and detector assembly. This is an improvement but leads to relatively slow measurements since the rather massive assembly cannot be moved rapidly. For measurements of stress as a function of temperature it is highly desirable for the scan to be extremely rapid so that continuous heating at various rates can be used.

It is possible to construct an apparatus in which laser, sample and detector are all stationary, as shown in Fig. B1. The galvanometer driven mirror provides a rapid scan in angle; it is converted by the long focal length lens into a linear scan across the wafer. The position of the reflected beam in the focal plane of the lens depends only on the angle of the reflected light relative to the optical axis. This arrangement has the same derivative measuring property as the simpler system; if a perfectly flat wafer is scanned, the reflected spot at te detector is stationary. As shown in the figure, a more compact system is obtained by folding the optical path with the addition of the fixed mirror.

The motion of the reflected spot in the focal plane of the lens is measured with a position sensitive photodiode. This may be considered as a sheet of uniform resistivity with a current source at the position of the light spot. The current is thus divided between the connections at the edges of the detector inversely as the distances from the spot to the edges. The position of the spot is then calculated as the ratio of the differences of these two currents to their sum; variations in light intensity affect numerator and denominator equally and do not change the result. For the actual measurement, the currents are amplified, converted to digital form and entered into a computer. The arithmetic is carried out digitally in the computer. The precision of the current measurement, determined by the resolution of the digital to analog converter, is 1 part in 2^{12}; after the arithmetic, the precision of the position of the beam should be about 1 part in 2^{11}. Since the width of the detector is about one centimeter, the position sensitivity is about 5 μm. With a path length of one meter, and the fact that the angle of the reflected beam changes twice as fast as the angle of the wafer surface, the instrument has a deflection sensitivity of about 2.5 microradians. For a sample of 100 mm diameter, this corresponds to a radius of curvature of 40 kilometers.

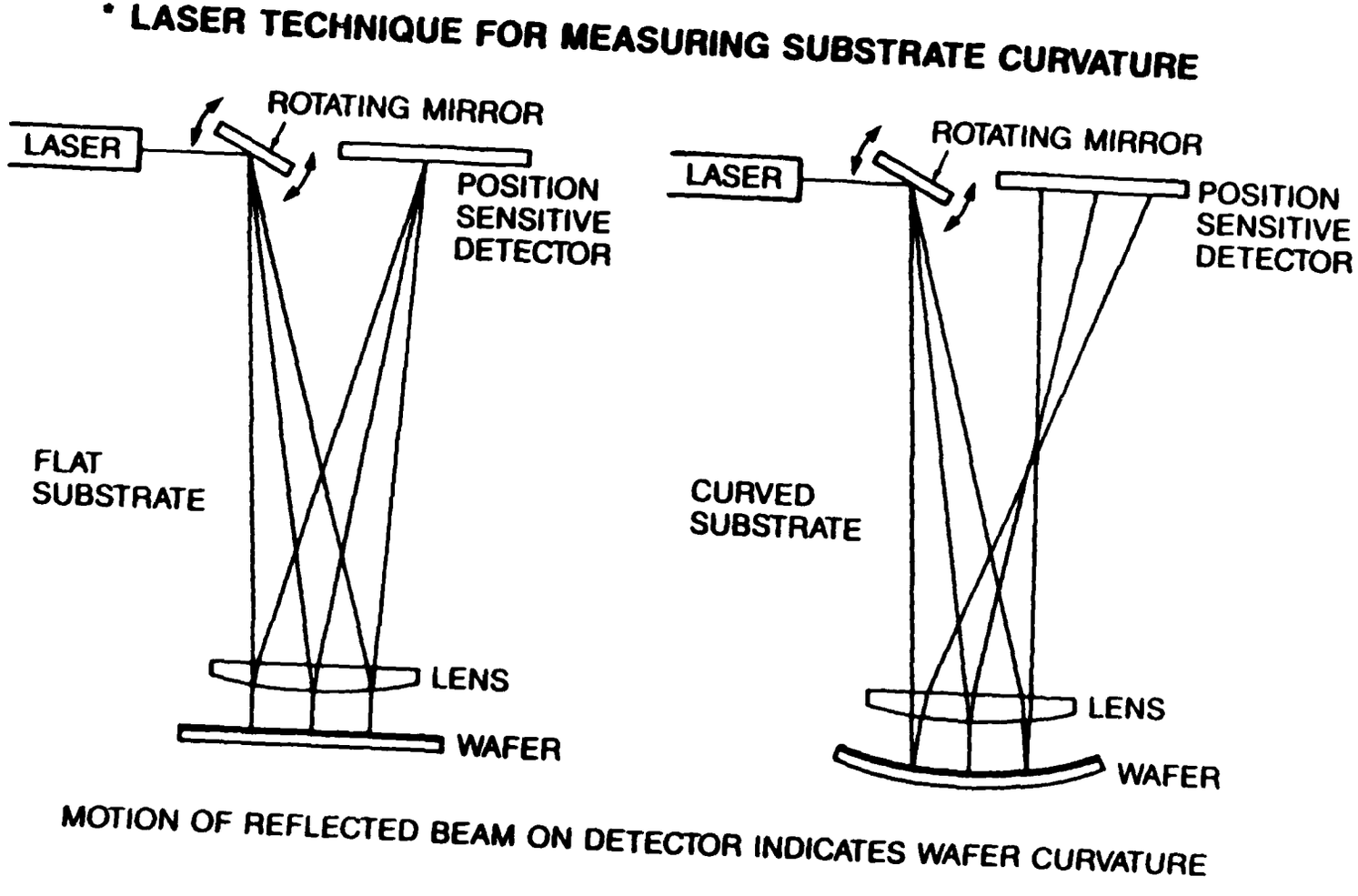

Fig. B1 Schematic illustration of laser system for measuring substrate curvature and stresses in thin films on substrates.

In operation, the wafer is scanned by the beam forward and backward across the wafer, with data taken at 25 points. The results of the scans of bare silicon wafers indicate that the wafers are not flat; consequently, a differential method must be used. The results of a bare wafer reference scan are subtracted, point by point, from the coated wafer data to remove the effects of both average curvature and local unevenness. The bare wafer measurement may be carried out either prior to deposition or after stripping the film. No permanent shape changes in silicon under the conditions normally used for rear end processing have been observed. For the differential technique to be effective it is necessary that the same points on the wafer be used for both measurements. This is accomplished by aligning the reference flat of the wafer with a reference line on the stage, and the use of an edge finding routine in the scanning procedure. The slope of the line for the difference data is determined by least squares fitting. It is proportional to the inverse radius of curvature, and the proportionality constant is determined by measurement of a spherical mirror of radius 10 meters, accurate within 3%. In practice, a precision of about $2*10^{-4}$ m^{-1} in 1/R is easily obtained. For typical films, this corresponds to a precision in stress of a few MPa.

The bending of a wafer under the force of gravity is measurable. For a typical 1 μm film on a 100 mm wafer supported first at the edge and then at the center, the stress change is about 50 MPa. On thermal cycling, the stress changes from tensile to compressive and back so that a wafer on a flat stage would change support point and be subject to the gravity effect. To eliminate the effect, the wafer is supported by three pins so that the curvature due to gravity is constant, and its contribution is eliminated by the subtraction procedure.

An electrically heated stage provides the capability for stress versus temperature measurements. A thermally insulating plate provided with a narrow slit for the laser beam is mounted above the wafer to minimize heat loss. A fan is needed to prevent accumulation of heated air in the optical path; otherwise, fluctuations in the refractive index of the heated air due to convection currents cause substantial deflections of the laser beam and serious noise in the measurements. In the present form of the apparatus the

sample can only be heated in air. Enclosing the sample to permit use of a controlled atmosphere would be possible, but it would be difficult to suppress the convection problem within the furnace chamber, and a window of extremely high optical quality would be needed to avoid loss of precision. The approximate temperature of the wafer is measured with a chromel-alumel thermocouple; the thermocouple signal is amplified and converted to digital form for computer input. The computer, under programmed control, adjusts the power to the heater so as to maintain any specified heating or cooling rate or isothermal hold. The present apparatus has a maximum heating rate of about 20 degrees per minute and can reach a maximum temperature of about 800° C. Since the stress measurement scan requires only a few seconds, continuous heating and cooling can be used; it is not necessary to hold and stabilize the temperature for each measurement. The stage has provision for internal forced air cooling so that reasonable cooling rates can be maintained as room temperature is approached.

The variation of stress with temperature for a typical Al-1%Si film sputtered at (nominally) room temperature is shown in Fig. B2. Initially the film is in a state of moderate tension. On heating, the tension decreases linearly with increasing temperature, with a slope of about -2.3 MPa/°C, down to a value of zero at about 50° C; then the stress becomes compressive, with the slope gradually decreasing. The compressive stress becomes a maximum at about 125° C, then decreases fairly rapidly to a low value at about 250° C that remains roughly constant with further heating. On cooling, there is a short linear regime with a slope about the same as that observed at the beginning of heating. On further cooling, the stress again becomes tensile, and the slope changes to a lower value that remains roughly constant down to room temperature. The detailed shapes of portions of the heating and cooling curves are weakly dependent on the heating and cooling rates.

Between the heating cycles, the sample relaxed at room temperature, so that the stress at the beginning of the second heating was substantially lower than it was immediately after cooling. On the second heating cycle, the first part of the curve is parallel to that observed on first heating, but no drop in stress occurs until nearly 200° C is reached. After the maximum tensile stress is reached, the stress decreases approximately linearly with increasing temperature. The curve for the second cooling is almost identical

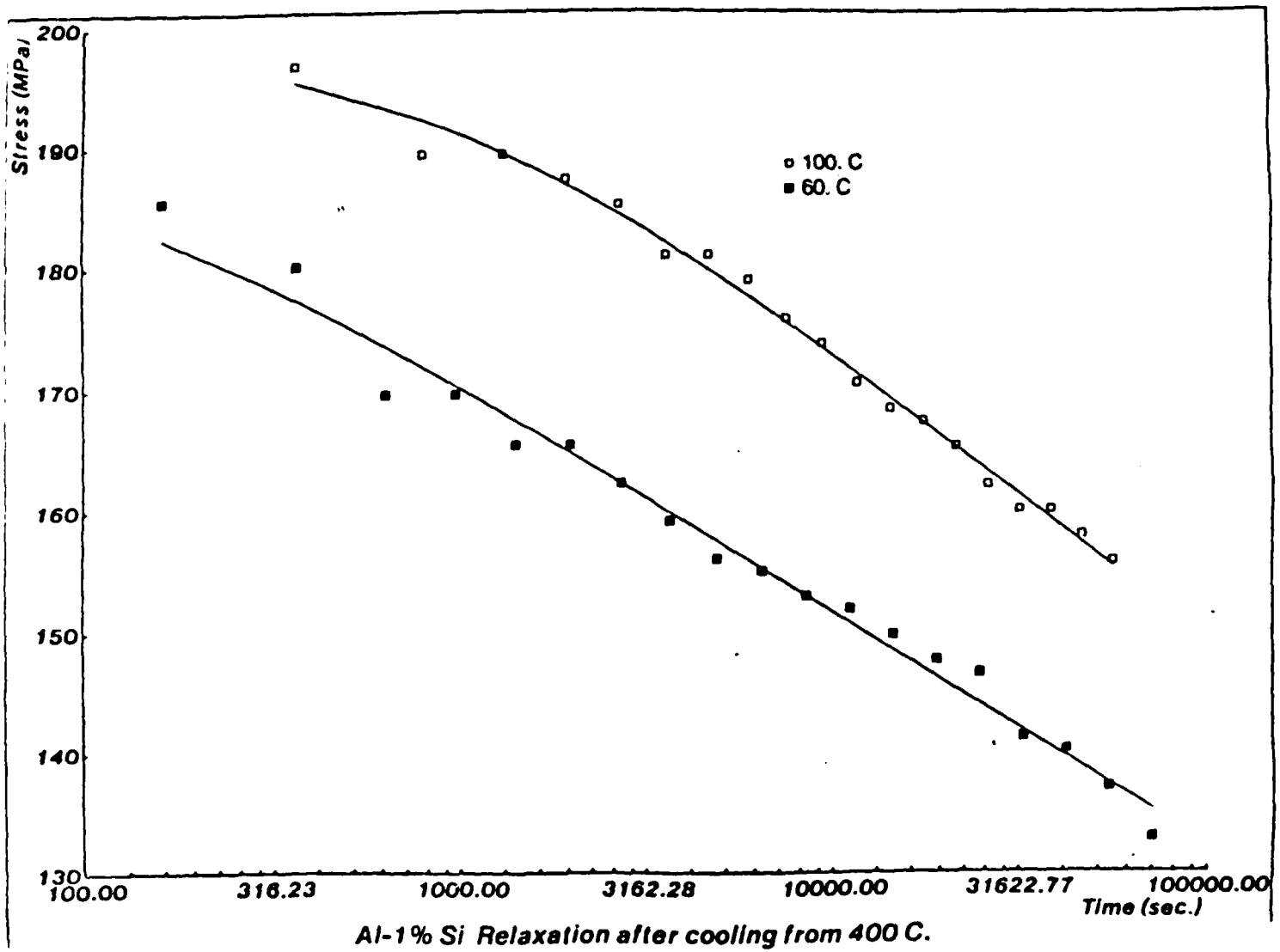

Fig. B2 Variation of stress with temperature for a typical thin film of Al+1%Si on an oxidized silicon substrate. The film was deposited at room temperature by sputtering.

with that for the first cooling. If the same heating and cooling rates are used, almost exactly the same curves are obtained on succeeding cycles.

The qualitative features of these curves can be readily understood. The initial heating region is one in which the aluminum behaves elastically; the slope can be calculated from the known properties of the materials. The initial stress is tensile as a result of cooling from the effective deposition temperature. (Sputtering normally produces some heating of the wafer.) The stress versus temperature curve on heating should be close (and parallel) to the curve for the behavior of the sample on cooling after deposition. In general, the curves will not be identical because significant stress relaxation can occur at room temperature and the stress at the beginning of our measurement is lower than that present immediately after deposition. The temperature at which the stress falls to zero on heating is, therefore, somewhat below the effective deposition temperature.

The decrease in the slope of the stress versus temperature curve as the stress becomes increasingly compressive indicates that the elastic range has been exceeded; plastic flow of the aluminum is occuring. The rapid drop in stress on further heating (only during the first heating) is due to recrystallization and grain growth. The aluminum crystallites in the material as sputtered are substantially smaller than the film thickness; during this portion of the first heating cycle crystal growth occurs until the crystal size is approximately equal to the filmthickness, and the rearrangement of atoms which occurs duing this process permits almost complete stress relaxation. Once the crystallite size reaches the film thickness, the structure is metastable and further changes normally do not occur.

Isothermal stress relaxation tests can be done on either the heating (compressive) or the cooling (tensile) portion of the curve; two examples are shown in Fig. B3. The curves are fit by a model that presumes a temperature dependent matrix of obstacles to dislocation motion which can be overcome by thermal activation and applied stress. Preliminary tests on 1 μm aluminum films indicate that the films relax about an order of magnitude slower than bulk samples under similar conditions.

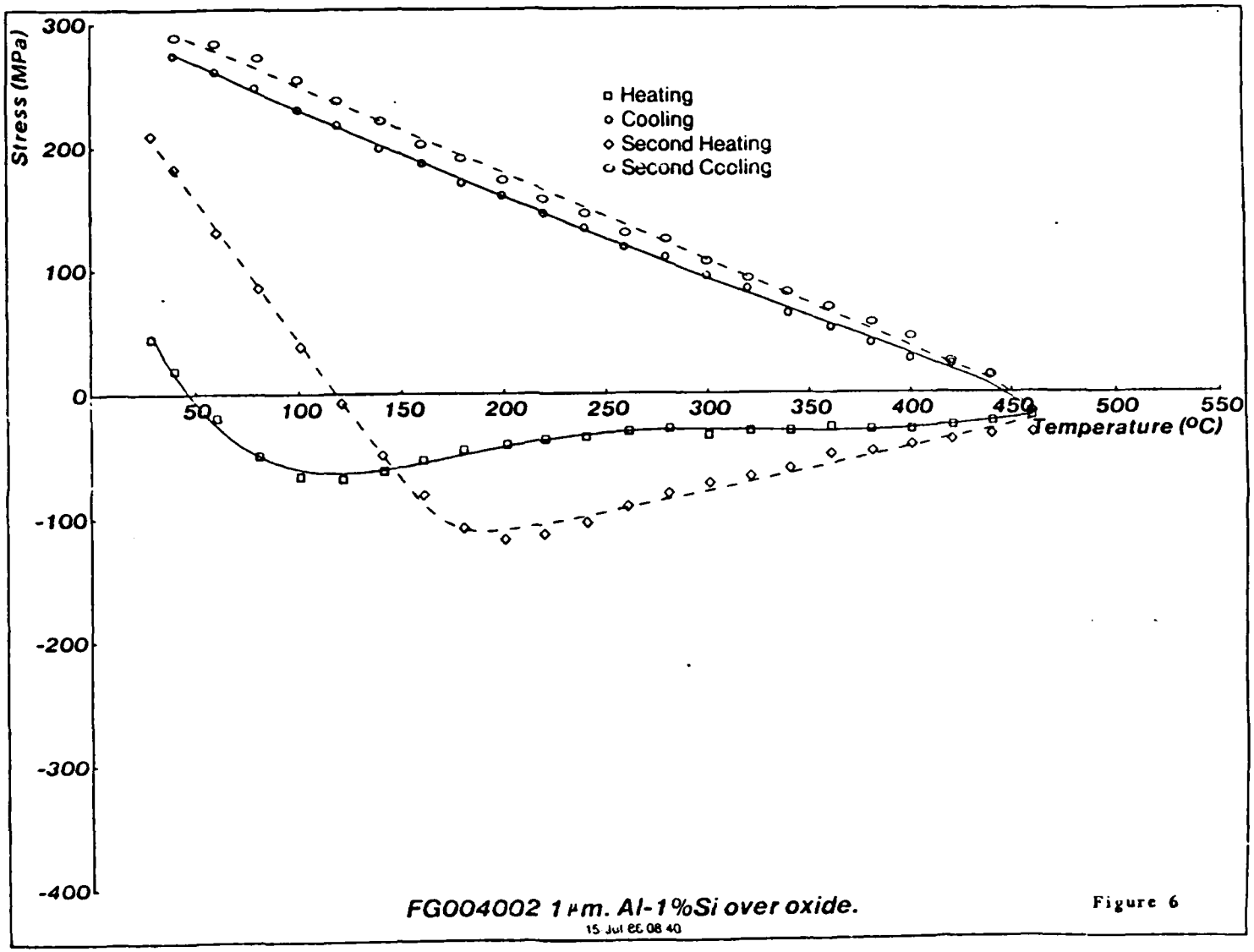

Fig. B3 Issothermal stress relaxation data for Al+1%Si on an oxidized silicon substrate.

Several factors influence the mechanical behavior of thin films and will be studied further. For example, submicron films of pure aluminum have been seen to sustain stresses twice those of the 1 μm Al-1%Si films; thus the effects of composition and film thickness will be studied. In addition, studies are planned to examine the effects of grain size and the presence of additional films.

C. Comparison of the Mechanical Properties of Thin Films as measured by Indentation and Substrate Curvature Techniques
(M.F. Doerner and W. D. Nix)

1. Introduction

Interest in the mechanical properties of thin films has been accelerating recently due in a large part to concern over the reliability of metallizations used for integrated circuit interconnections. Knowledge of the mechanical strength of the materials used for these interconnections is important to an understanding of the failure mechanisms and to obtaining the appropriate solutions. Two common techniques used in the study of thin film mechanical properties are substrate bending techniques [1-6] for detecting stresses in thin films and sub-micron indentation techniques [7-10]. In this section of the report we describe the application of both methods to the determination of the strength of two materials used for metallizations: aluminum and tungsten.

2. Hardness

Hardness results for the as-deposited aluminum films as a function of indentation depth are shown in Fig. C1. The hardness is seen to increase as the depth of indentation approaches that of the film thickness, due to the presence of the harder substrate. For soft materials on a hard substrate, a depth to film thickness ratio of 1/4 or less is required to obtain hardness values independent of the substrate [7,11]. Hardness data for tungsten films as a function of indentation depth are plotted in Fig. C2. In this case, the silicon substrate is somewhat softer than the film (hardness=14.2 GPa for silicon). A significant decrease in hardness is observed only for indentations deeper than the film thickness. For these reasons, the hardness values quoted later for W and Al will be those taken at a depth/thickness ratio of 1/4. Also, the hardness values for aluminum decrease with annealing as expected, as shown in Fig. C3.

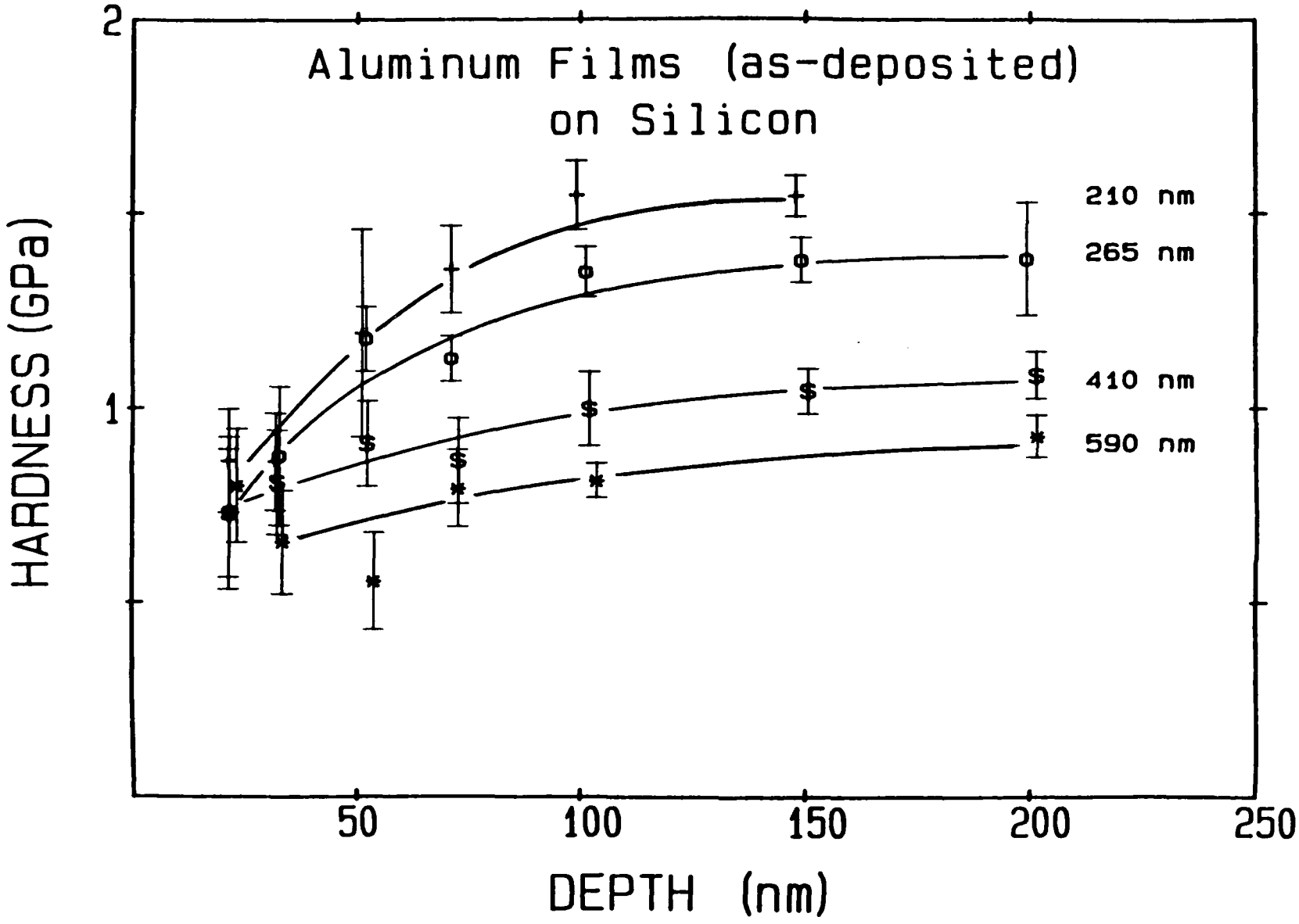

Fig. C1 Hardness results for the as-deposited aluminum films on silicon substrates as a function of indentation depth. Error bars are ± 1 standard deviation for 4 measurements.

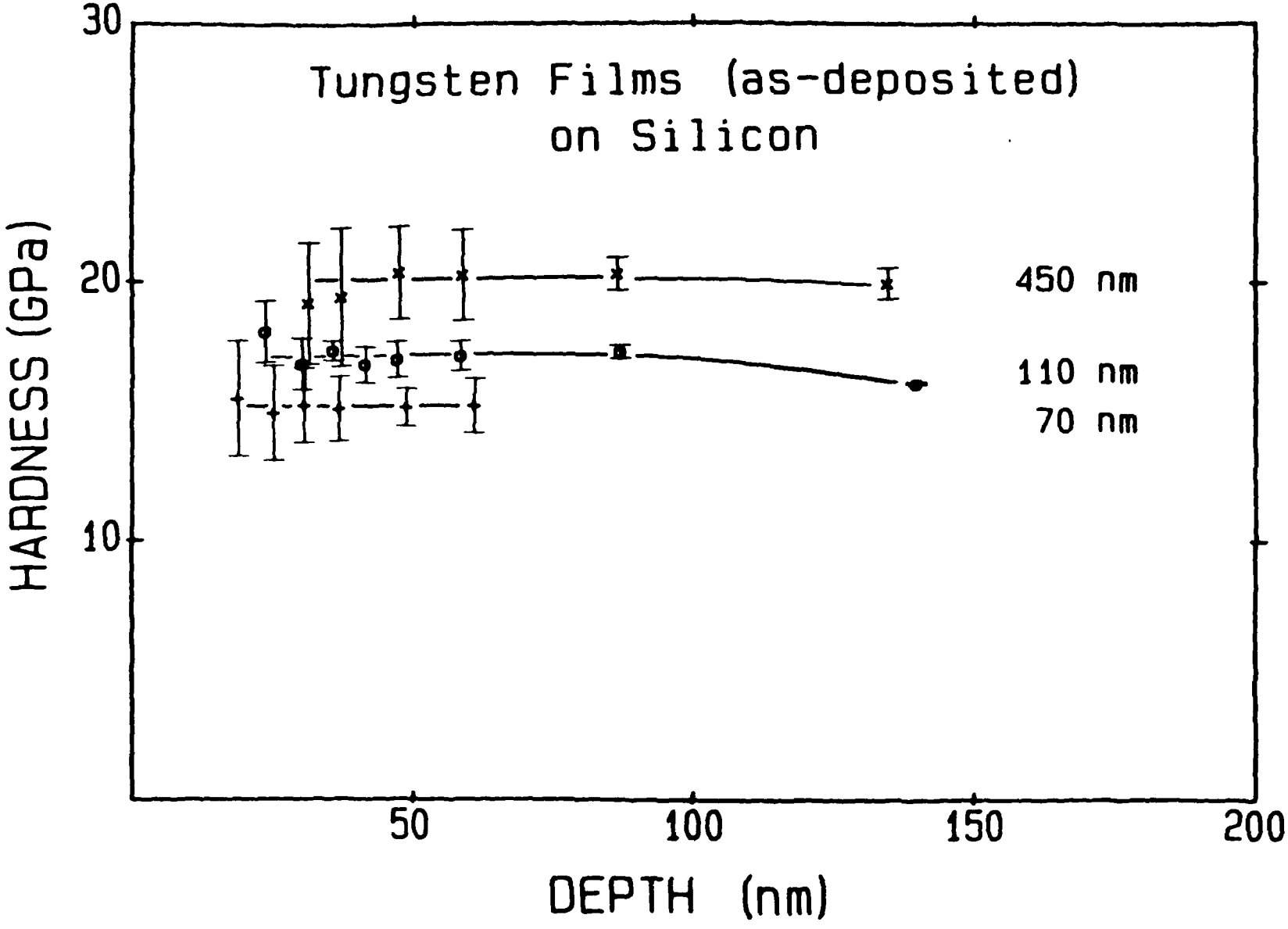

Fig. C2 Hardness results for the as-deposited tungsten films on silicon substrates. Error bars are ± 1 standard deviation for 4 measurements.

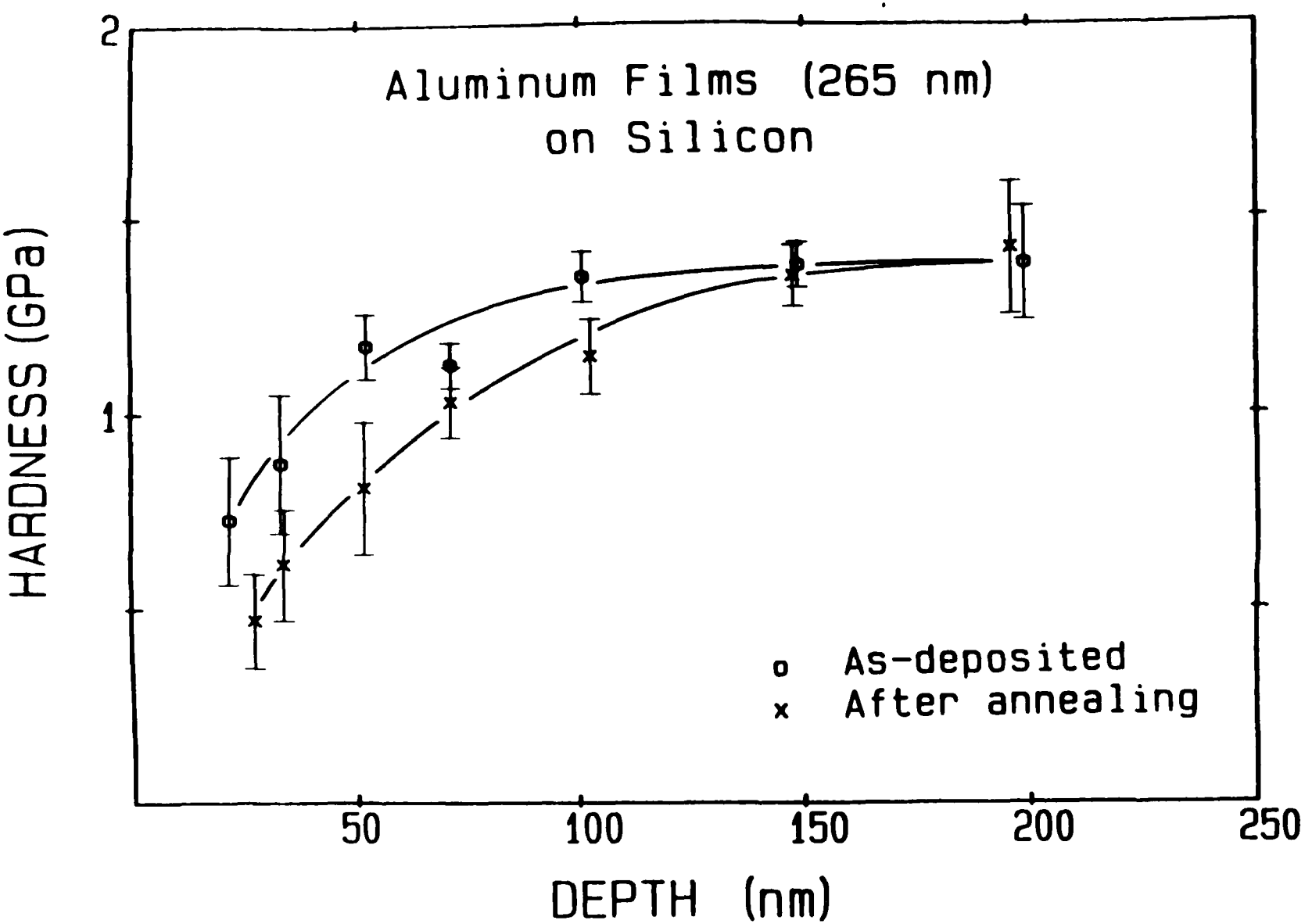

Fig. C3 The effect of annealing on the hardness is illustrated for a 265 nm thick aluminum film. The film was annealed in the substrate curvature apparatus by heating and cooling at 6°C/minute (maximum temperature 723K).

3. Substrate Curvature

Examples of stress/temperature results for aluminum films 210 and 590 nm thick are shown in Fig. C4. During initial heating significant microstructural changes occur in the aluminum (as is evident from the hardness data). Significant grain growth has been observed to occur on annealing as-deposited aluminum films [2]. These changes in the microstructure result in a significant stress drop beginning around 373K for the first heating. The results shown in Fig. C4 were obtained for the second heating after the microstructure had stabilized (additional cycles give identical results).

After the first heating cycle, the aluminum films at room temperature are in biaxial tension due to the deformation which has occurred in compression at high temperature. During the second cycle (referring to Fig. C4), initial heating results in a linear decrease in the stress according to

$$\frac{d\sigma}{dT} = \left[\frac{E}{1-\nu}\right]_{film} \Delta\alpha$$

where $\Delta\alpha$ is the difference in thermal expansion coefficients for the film and substrate. In this region, the film is deforming elastically and the stress level is not an indication of film strength. However, as the stress becomes increasingly compressive, the film begins to deform plastically and a plateau in stress is observed. This stress level decreases slightly with increasing temperature indicating a decreasing flow stress with increasing temperature. On cooling, an elastic region is first observed followed by plastic deformation until the film returns to its initial state of biaxial tension at room temperature. The stresses measured at room temperature during cooling and at high temperature during heating are the flow strengths of the films since the films are plastically deforming in these regions.

As illustrated in Fig. C4, the film thickness has a significant effect on the plastic resistance of the film at both high and low temperature. The strength of the film with a

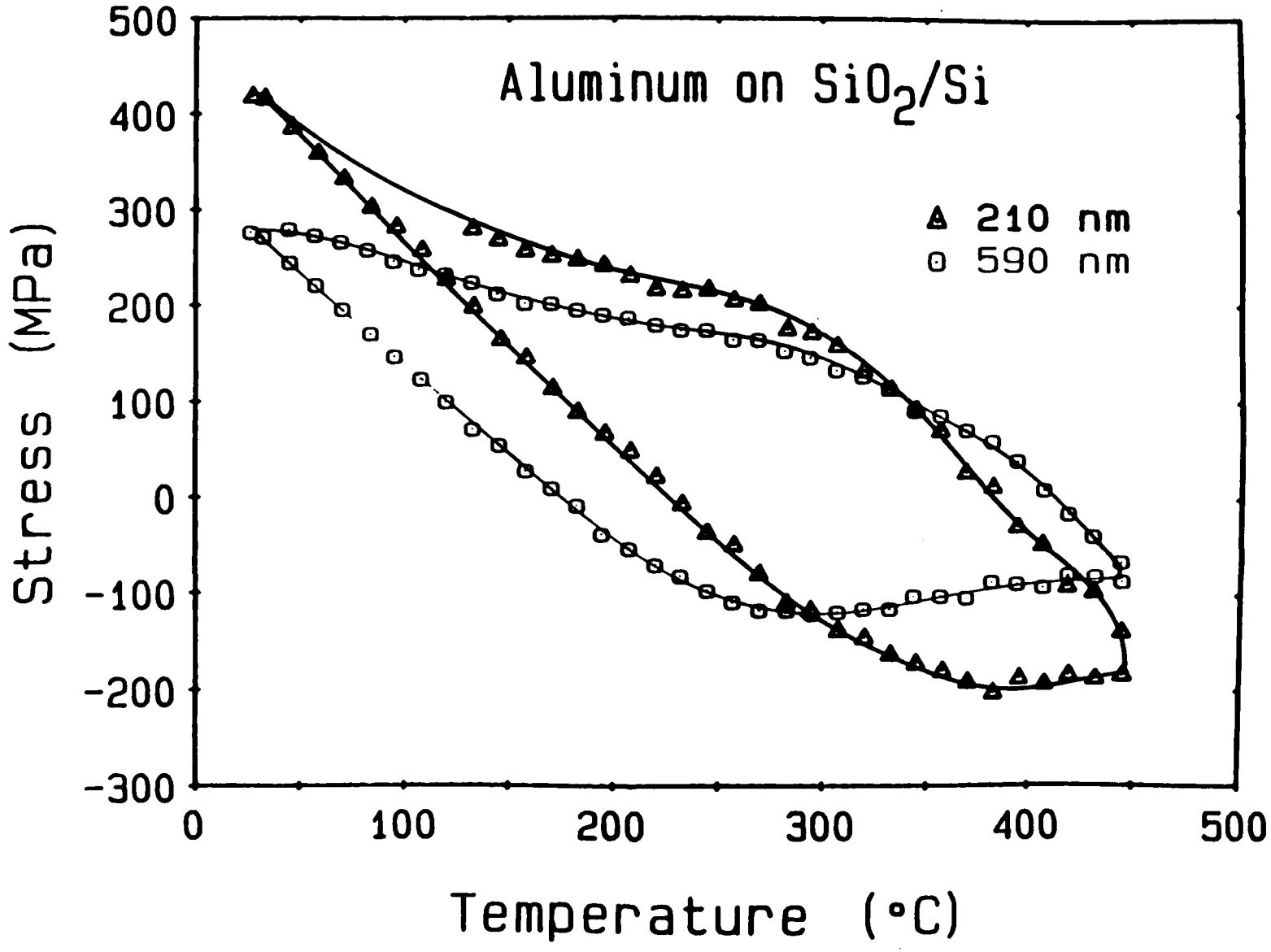

Fig. C4 Stress measurements from the substrate curvature apparatus for aluminum films of two different thicknesses. Data are for the second heating cycle.

thickness of 210 nm is significantly greater than that of the 590 nm thick film both at high temperature in compression and at low temperature in tension. The observed stress levels at 318K during cooling are plotted against film thickness in Fig. C5. This temperature, slighty above room temperature, was chosen since it was difficult to maintain the specified cooling rate near room temperature. The hardnesses of the annealed films at a depth of 1/4 the film thickness are also shown. Both techniques show an increasing film strength with decreasing thickness. This trend is in agreement with the results of Sinha and Sheng [2] for evaporated aluminum films, although they found a much larger thickness dependence (strength varied by a factor of 8 over the thickness range considered here).

The tungsten films, for the deposition conditions used, were deposited with very high intrinsic compressive stresses. These stresses are a result of the "shot-peening" action of neutral and charged argon atoms reflected from the target onto the growing film. Since the probability of elastic reflection is increased as the atomic mass of the target increases [12], this bombardment of the film is much greater for tungsten than for aluminum. The compressive stresses generated for these tungsten films were high enough to cause plastic yielding of the as-deposited films. The fact that the films are at their yield stress in the as-deposited condition was determined by heating a film in the wafer curvature apparatus, and noting that the compressive stress did not increase as the temperature increased. An increase in the compressive biaxial stress would be expected if the film were deforming elastically. The as-deposited stress in the film is therefore the yield strength of the film. The as-deposited stress is plotted along with the hardness as a function of film thickness in Fig. C6. For the tungsten films, the dependence of the flow strength on film thickness is opposite to that found for aluminum; the film strength increases with increasing film thickness.

4. Thickness Effects on Strength

In the case of aluminum, it is possible that part of the observed thickness effect on strength is due to microstructural variations with film thickness. The grain size of the annealed films (measured only for the thinnest and thickest films) scales with the

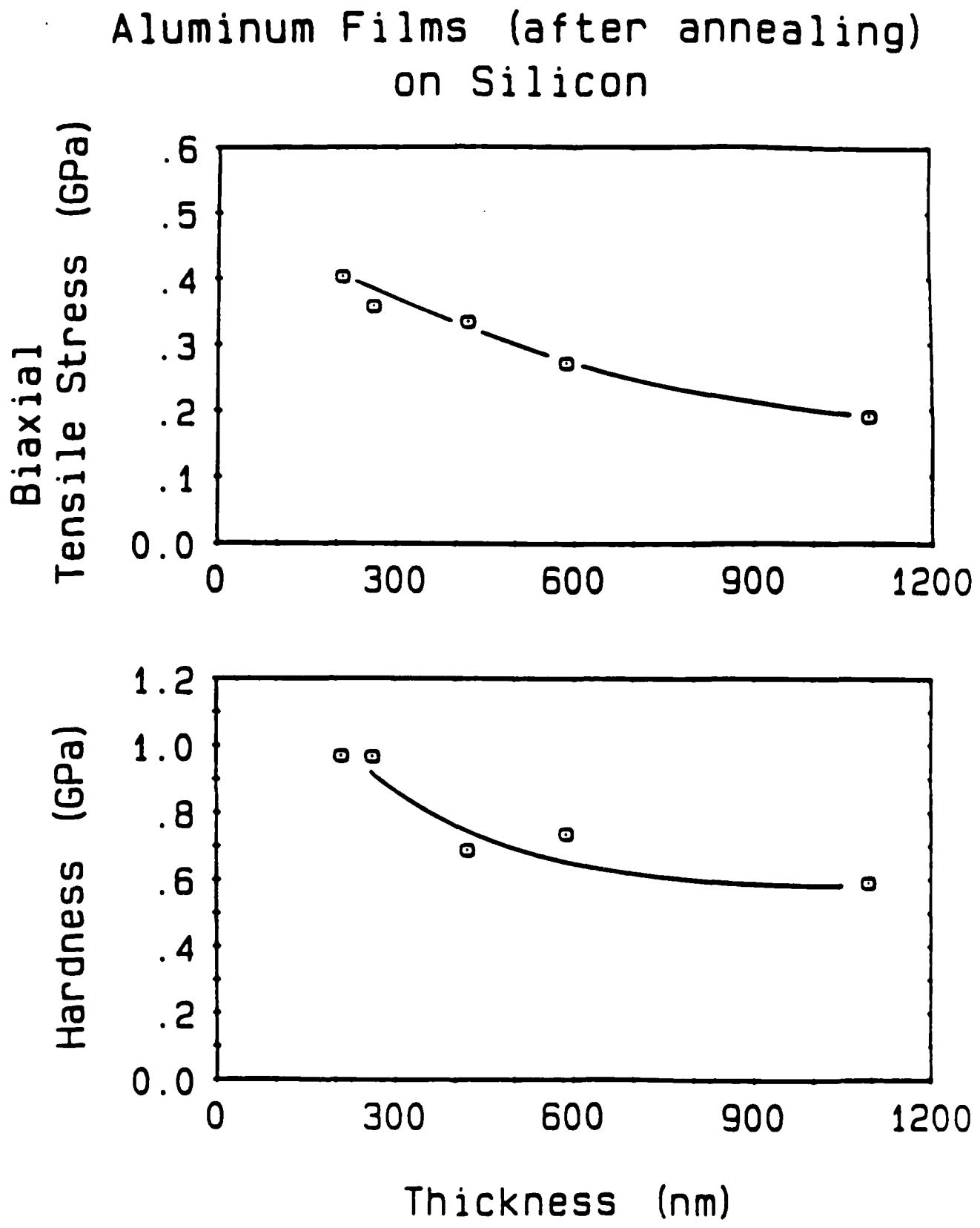

Fig. C5 The biaxial yield stress and hardness as a function of film thickness for aluminum films on silicon substrates. The plastic strength decreases with increasing film thickness.

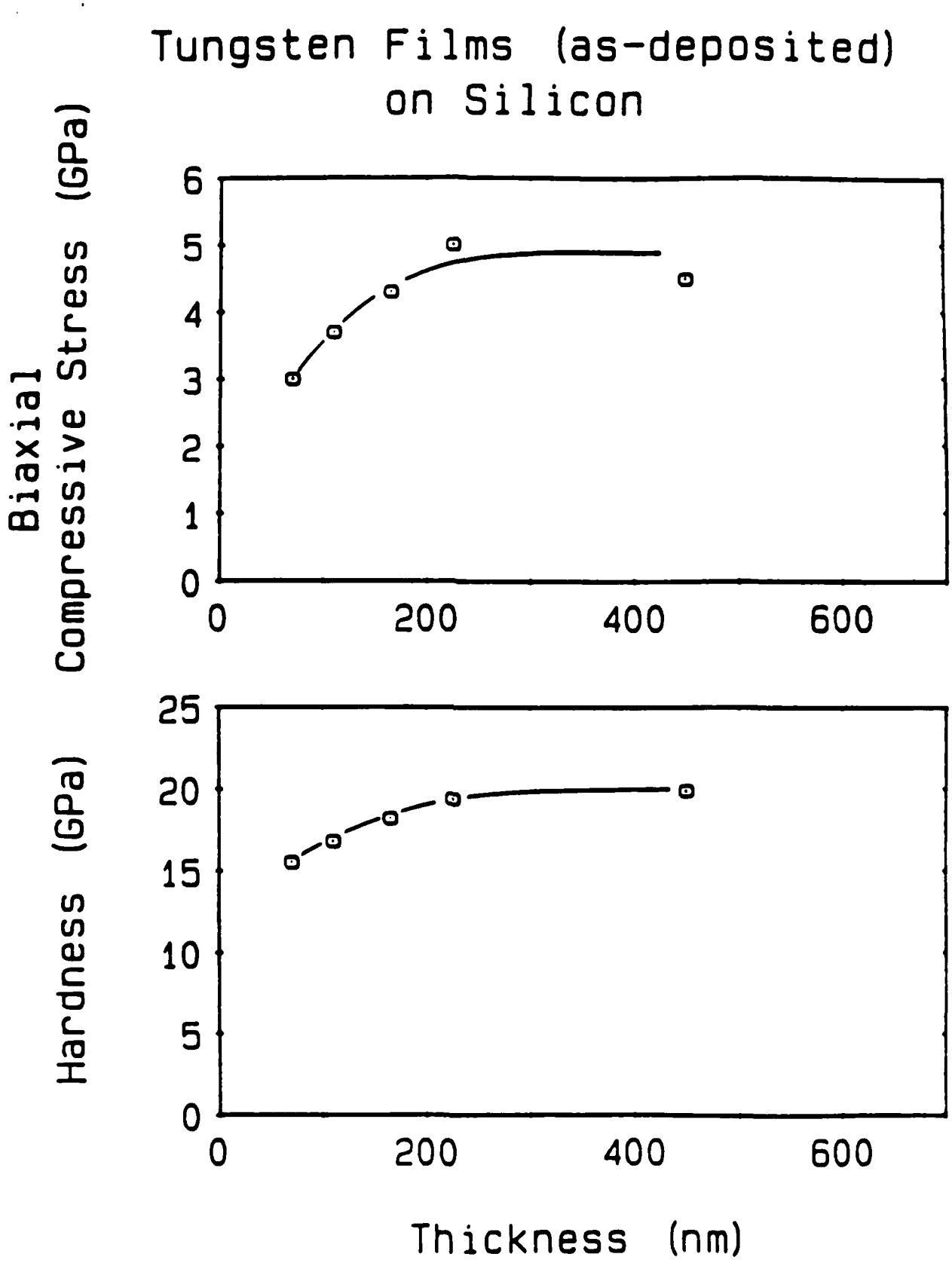

Fig. C6 The biaxial yield stress and hardness as a function of film thickness for tungsten films. The plastic strength increases with increasing film thickness.

thickness. If this grain size/thickness relationship is interpolated for the films of intermediate thickness, the stress data can be plotted assuming a Hall-Petch relationship as shown in Fig. C7. This analysis gives a Hall-Petch slope of 20×10^4 N/m$^{3/2}$ and an intercept of 42 MPa. Values of the Hall-Petch slope for bulk aluminum [13,14] range from 4×10^4 to 8×10^4 N/m$^{3/2}$ with intercepts from 5 to 16 MPa. Assuming the results of bulk aluminum can be extrapolated to the much smaller grain size present in thin films, it appears the thickness strength effect is much larger than that expected from the microstructure.

It is interesting to consider that the aluminum film strength at high temperature (3/4 T_M) is also inversely dependent on film thickness. At high temperature, the smaller grain size would normally be expected to weaken the film due to the operation of grain boundary sliding and diffusion mechanisms. The formation of hillocks during high temperature annealing of these films suggests that these mechanisms occur. However, as seen in Table I, the thicker films show the largest displacements of the surface relative to the grain size (6% of the grain size for the thinnest film and 20% of the grain size for the thickest film). This result is opposite to what would be expected from the grain size considering that the rates of grain boundary sliding and diffusion should be highest for the films with smaller grain size. In addition, the thinnest films are subjected to the highest stresses since less plastic deformation has occurred at low temperature during heating. It appears that grain boundary sliding and diffusion are somehow suppressed for the thinner films. It has been suggested [15,16] that dislocation slip is required to nucleate hillock formation. If this is the case, the mechanism responsible for the increased strength of the thin aluminum films may be the same at both low and high temperature.

The effect of image forces on dislocations in the film due to the presence of the substrate and oxide phases of differing elastic properties may also play a role in thin film strength. For aluminum, results of the wafer curvature and hardness data suggest the presence of the substrate strengthens the film. In this case, the shear modulus of the substrate is higher than that of the film. In the case of tungsten, where the substrate is elastically less stiff than the film, the opposite result is observed.

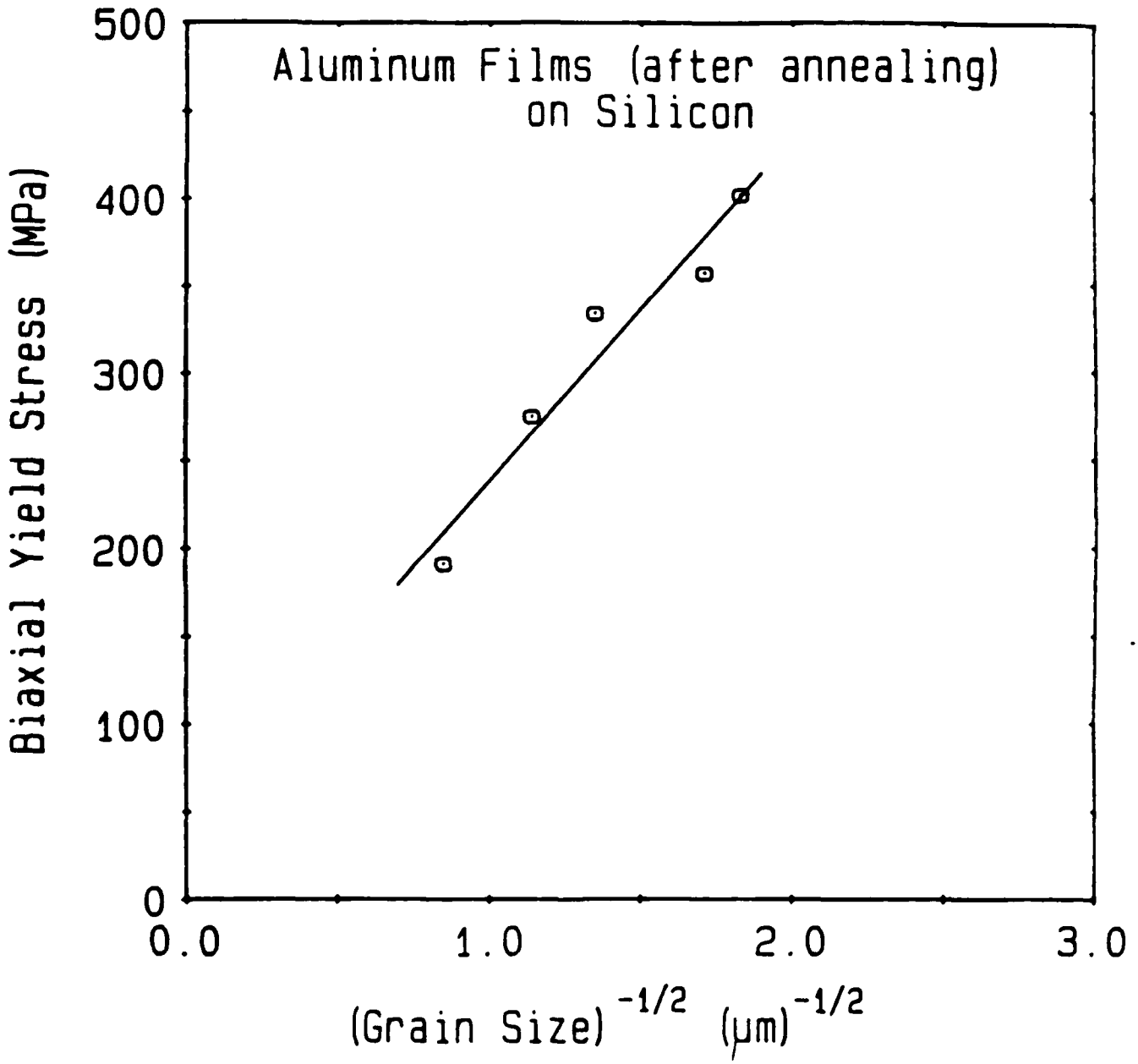

Fig. C7 Hall-Petch plot of the biaxial yield stress for annealed aluminum thin films. Grain size measurements were made for the largest and smallest grain sizes only. The intermediate grain sizes were interpolated using the film thicknesses.The slope obtained is 20×10^4 N/m$^{3/2}$ with an intercept of 42 MPa.

5. Summary

The effect of thickness on the strength of Al and W thin films on Si was studied using both substrate curvature and indentation hardness techniques. For Al, the film strength was found to increase with decreasing film thickness, whereas for tungsten, the strength decreases with decreasing film thickness. A comparison of the hardness to wafer curvature strength for both materials suggests that the strength of the film on the substrate differs from that of the film alone.

References

1. A. K. Sinha, H. J. Levinstein and T. E. Smith, J. Appl. Phys., 49, 2423 (1978)

2. A. K. Sinha and T. T. Sheng, Thin Solid Films, 48, 117 (1978)

3. P. H. Townsend and H. A. Vanderplas, Materials Research Society Symposia Proceedings, 47, 121 (1985)

4. M. Hershkovitz, I. A. Blech and Y. Komem,Thin Solid Films, 130, 87 (1985)

5. H. Hieber and T. Simon, Proceedings of International Reliability Physics Symposium, IEEE Electron Devices and Reliability Societies, 253 (1986)

6. C. K. Hu, D. Gupta and P. S. Ho, Proceedings 2nd International IEEE VLSI Multilevel Interconnect Conference, 187 (1985)

7. H. M. Pollock, D. Maugis and M. Barquins in Microindentation Techniques in Materials Science and Engineering, P.J. Blau and B. R. Lawn, Eds., ASTM, Philadelphia,PA , 47 (1985)

8. A. G. Dirks, J. J. Van den Broek and P. E. Wierenga, J. Appl. Phys., 55, 4248 (1984)

9. D. Stone,W. La Fontaine, S. Ruoff and C. Y. Li, Materials Research Society Symposia Proceedings , 72 (1986)

10. M. F. Doerner and W. D. Nix, J. Mater. Res.,1, 601 (1986)

11. D. Lebouvier, P. Gilormini and E. Felder, J. of Phys. D, 18, 199 (1985)

12. J. A. Thornton, J. Tabock and D. W. Hoffman, Thin Solid Films, 64, 111 (1979)

13. N. Hansen, Acta Met., 25, 863 (1977)

14. R. W. Armstrong in Advances in Materials Research Vol. 4, H. Herman Ed. Interscience, New York (1970)

15. M. Ronay and C. F. Aliotta, Phil. Mag. A, 42, 161 (1980)

16. P. Chaudhari, J. Appl. Phys., 45, 4339 (1974)

D. Elastic Interactions of Screw Dislocations in Thin Films on Substrates
(M.L. Ovecoglu, M.F. Doerner and W.D. Nix)

The study of dislocations in multiphase layered media provides a basis for understanding the mechanical properties of thin films. The close proximity of phases with different elastic properties can lead to image forces on dislocations within the film and these forces can influence the motion of the dislocations. A method for calculating the forces on dislocations in a thin film is therefore required. Here we report on recent progress we have made in calculating dislocation forces in thin films. Only a few of the results we have obtained will be given. The reader should consult the full paper on this topic for more details and results.

Previously, solutions have been obtained for relatively simple multiphase problems, most of which were based on multiple image analysis. We have also chosen the image method to calculate the elastic interactions because the method is direct and is extendable to problems with additional phases. As more complicated problems are considered, the image dislocation array can not be easily reduced to an infinite series, but must be expressed in terms of recursion formulae. In this investigation, we consider the image forces on a screw dislocation due to its interactions with nearby phases. We have extended the basic image solution and have solved the related image problems for a screw dislocation in a film for the following cases: two interfaces (due to substrate and free surface), three interfaces (due to substrate, film oxide and free surface), and four interfaces (due to substrate, substrate oxide, film oxide and free surface). We have also calculated the maximum shear stresses in the adjoining phases. These calculations permit a study of the yielding behavior in thin films as well as yielding or fracture behavior in the adjoining phases.

The infinite image solution for the four interface problem of a screw dislocation in a thin film with a surface oxide on an oxidized substrate was obtained by starting with the simplest case of one interface and systematically adding phases. Throughout the analysis, each phase is assumed to be elastically isotropic and perfectly welded to the others. A x-y-z right hand cartesian coordinate system is taken such that the y and z directions lie parallel to the interfaces between the phases. The calculations are based on the interactions of an infinitely long straight screw dislocation or that of a screw dislocation dipole which lies inside the film on a slip plane coplanar with the x-z plane. Schematic

illustrations of the multiphase image problems considered are given in Fig. D1. Here a, c, and t stand for the film, film-oxide, and substrate-oxide phase thicknesses, respectively. The substrate/film interface is located at $x = 0$ with the dislocation located at $x = x_0$. By separating the problem into four cases, it is possible to see how the solution can be obtained in a systematic way. Also, the influence of each additional phase on the dislocation interactions can be easily determined.

Numerical calculations based on the results of the multiple image analysis were performed for aluminum thin films of various thicknesses on an oxidized silicon substrate. The shear modulus and thickness values included in the calculations are those for an aluminum thin film, a silicon substrate, an SiO_2 substrate oxide and an Al_2O_3 film oxide. The image forces were calculated by including the effects of image dislocations for 5 iterations of the recursion relations.

1. One Dislocation Case

The total image force on a screw dislocation in the four interface case can be derived from the image solution. The image force on the real dislocation is calculated as the force due to the stress fields of all the image dislocations in the film solution.

The calculated results for the case of a screw dislocation in an aluminum thin film on silicon with a thin aluminum oxide layer at the surface (3 interface case) are shown in Fig. D2. Here R is the ratio of oxide thickness to film thickness. The effect of the surface oxide is to reduce the attractive force of the free surface. At a dislocation position close to the film/oxide interface, the image force becomes negative indicating a repulsion by the oxide layer. In this problem, in the absence of an applied stress, the dislocation will move to an equilibrium position close to the oxide where the image force is zero. As R decreases, the influence of the free surface becomes greater and the equilibrium position moves closer to the film/oxide interface.

The calculated results for the four interface problem are shown in Fig. D3. A silicon dioxide layer has been added between the silicon substrate and aluminum thin film. Since the shear modulus of the silicon dioxide is less than that of the silicon, a decrease in the image force near the substrate is observed in the four interface case. The effect of the

Image Problems for Screw Dislocations in Thin Films on Substrates

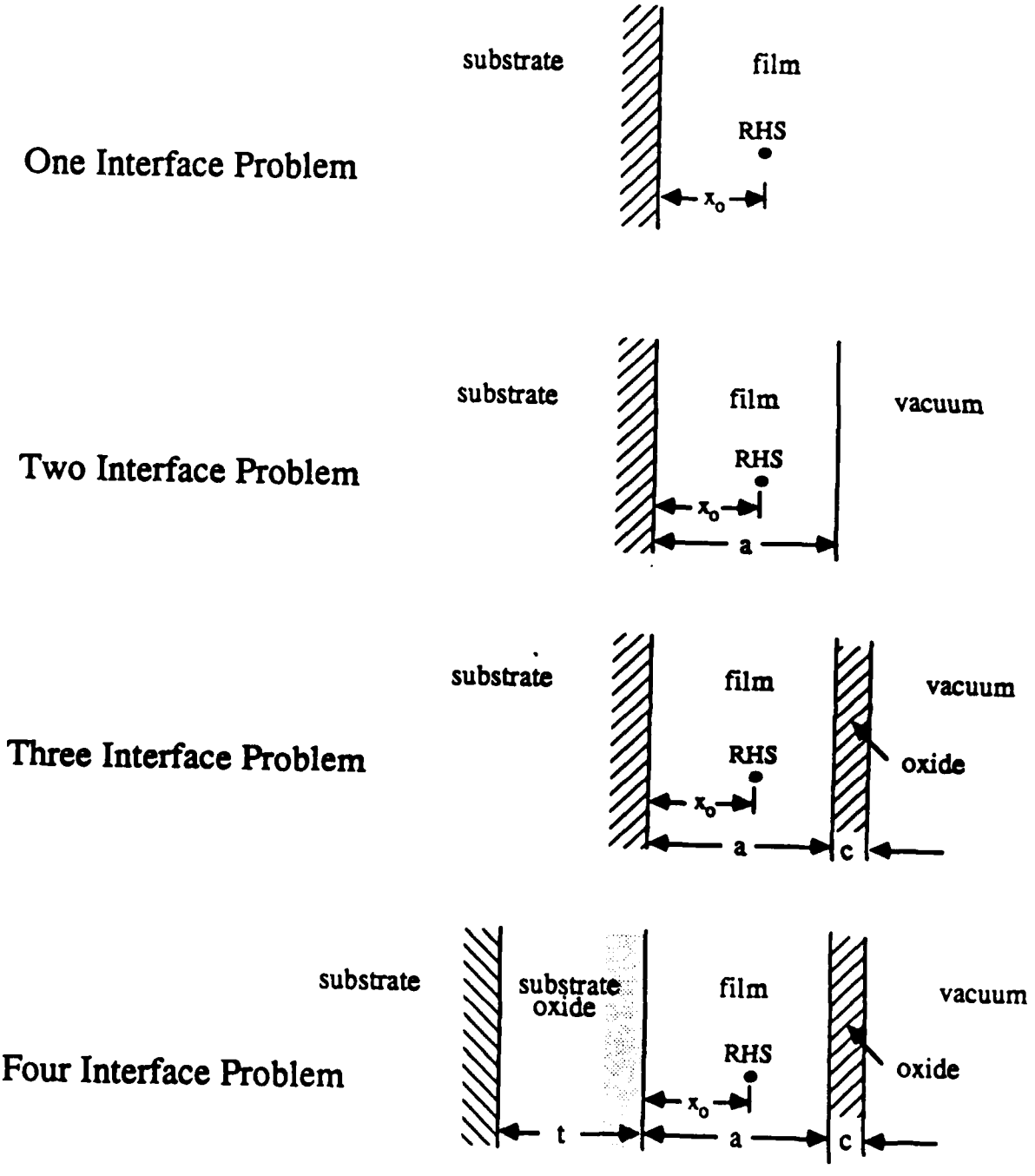

Fig. D1 Schematic illustration of the multiphase image problems.

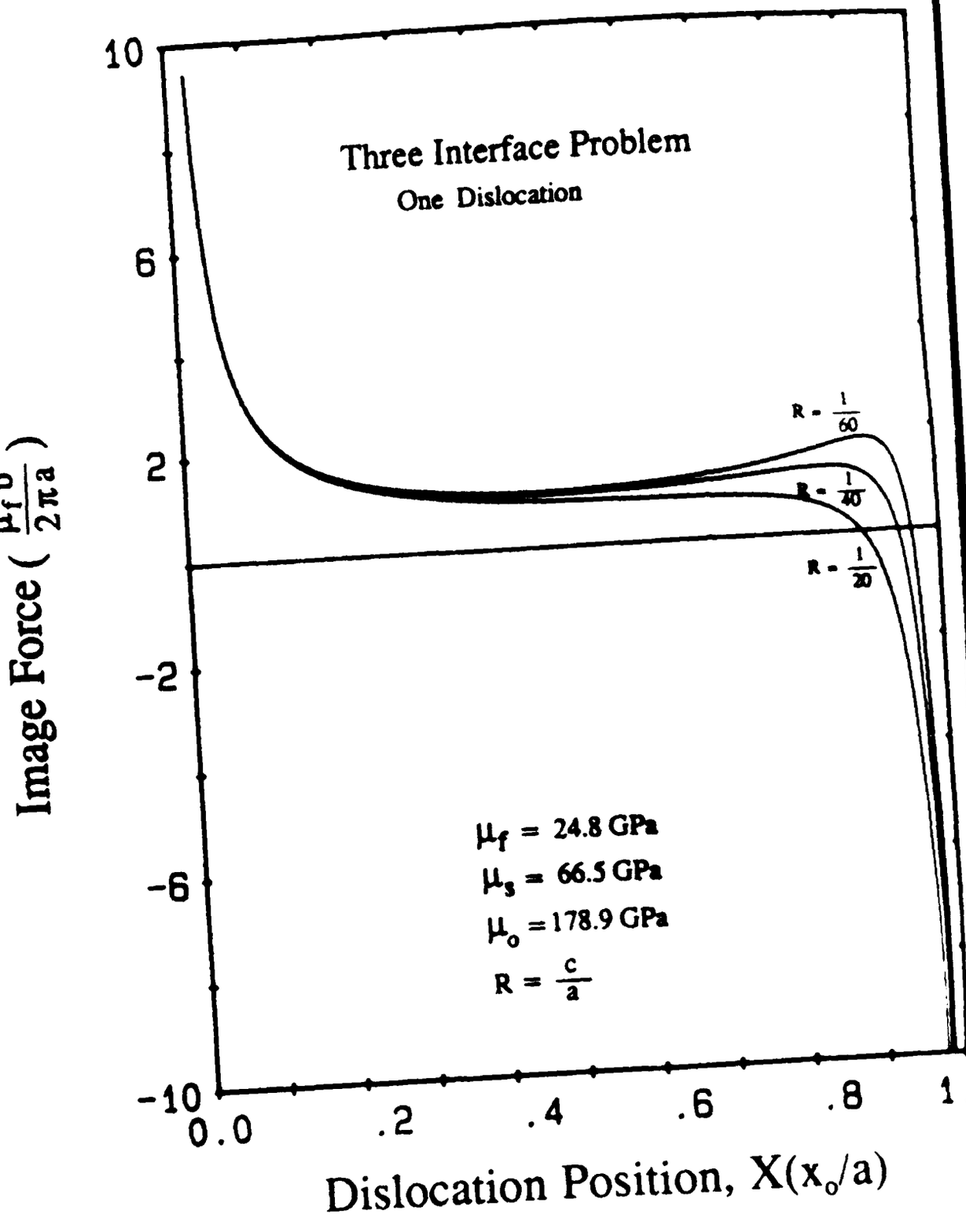

Fig. D2 Variation of the image force with dislocation position for a screw dislocation in the $Si/Al/Al_2O_3$ three interface case with a stiff oxide.

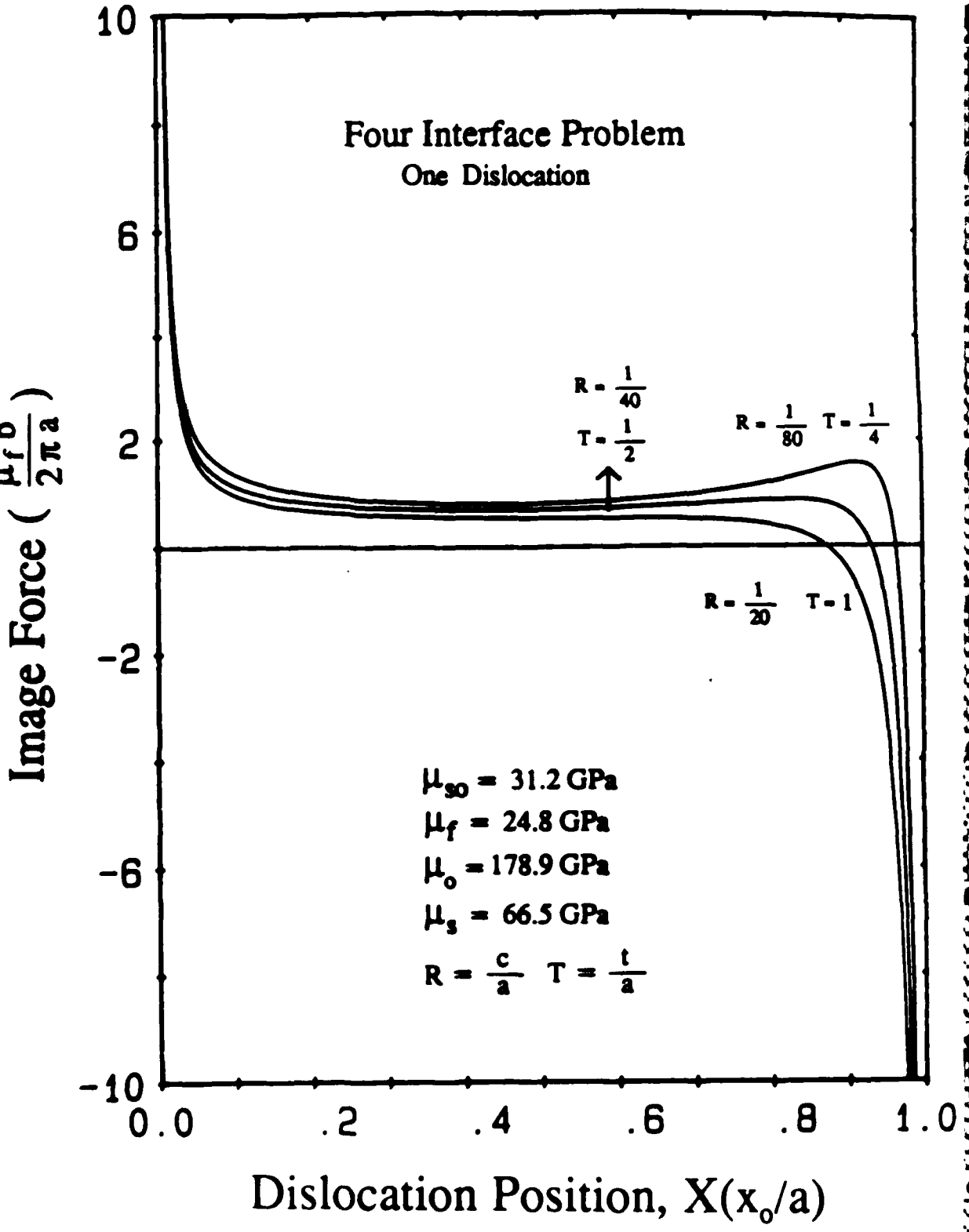

Fig. D3 Variation of the image force with dislocation position for a screw dislocation in the $Si/SiO_2/Al/Al_2O_3$ four interface case.

substrate oxide is less important for dislocation positions near the film/film oxide interface.

2. Dislocation Dipole

Calculations were also performed to determine the forces on two oppositely signed screw dislocations in the film on the same slip plane. The interaction forces between the two dislocations and the image forces were determined for the case in which one dislocation was held fixed with no applied stress, and for the case in which the dislocations were allowed to attain their equilibrium positions under an applied stress. In this way, a minimum stress to hold the dislocation pair apart was obtained.

A positive applied stress in the thin film would be required to hold the two dislocations at equilibrium positions near the interfaces. At equilibrium, the total force acting on each dislocation is zero. Using the same numerical method developed by Ovecoglu, Barnett and Nix[1], the equilibrium standoff distances are determined at different applied stress levels and plotted in Fig. D4.

3. Stresses in Adjoining Phases

Another important problem involves the calculation of the maximum stress in the adjoining phases due to the presence of a screw dislocation couple in the film. The determination of the maximum shear stresses in the adjacent phases due to the elastic fields of the image dislocations may be used to predict the onset of plastic flow or fracture in these phases. The maximum stresses in the adjacent phases due to the images of the real dislocations in the film, occur at the adjacent phase/film interface. The shear stresses at the interface with the adjoining phase can be determined from the stress fields of the image dislocations in that phase evaluated at the interface and $y = 0$.

The maximum stress in the film oxide due to the presence of an oppositely signed dislocation couple as a function of applied stress in the film is plotted in Fig. D5 for the three interface case. The major contribution to the oxide stress at all applied stress levels comes from the presence of the dislocation closest to the film/oxide interface . The stress in the oxide increases as the applied stress increases since this dislocation moves closer to

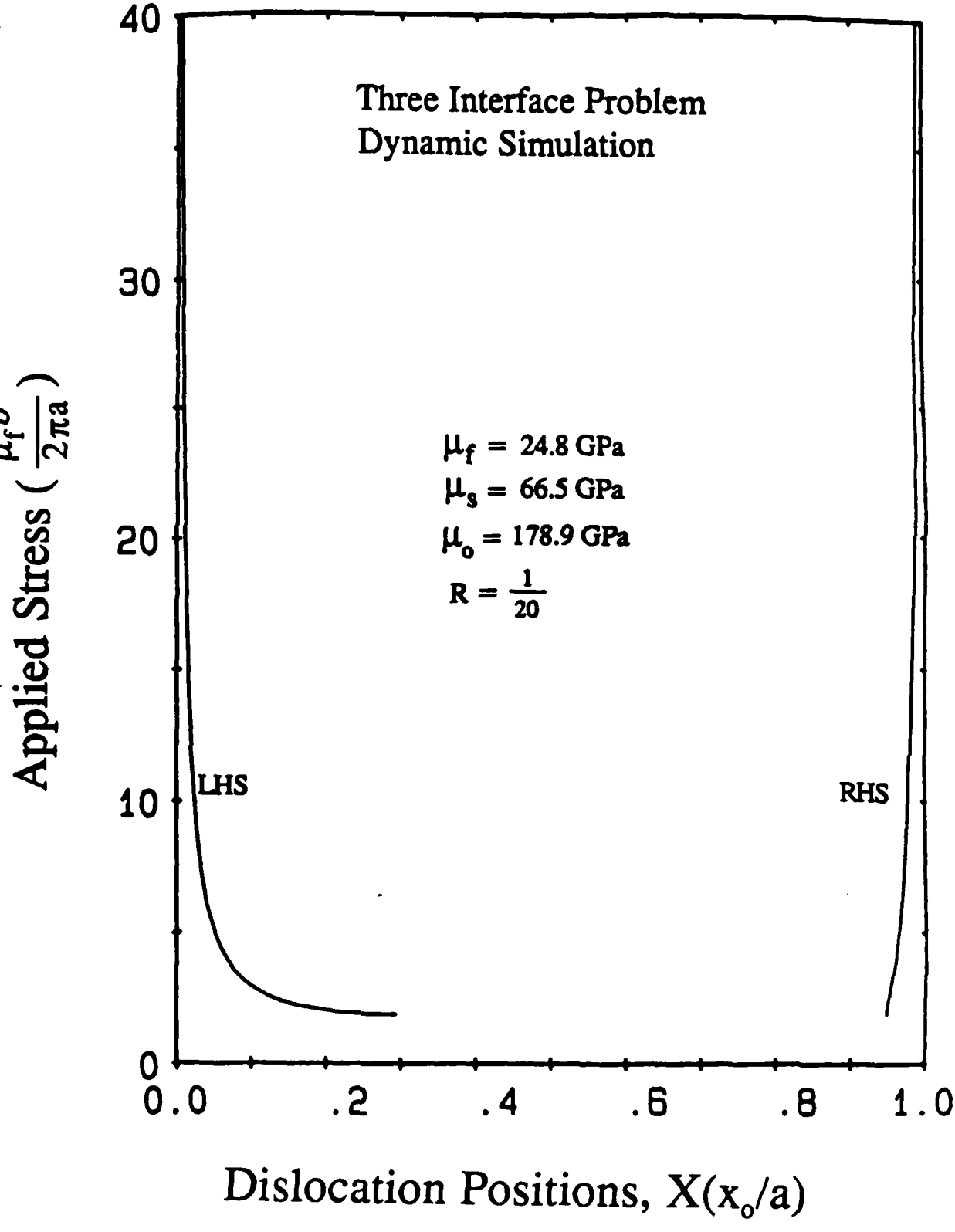

Fig. D4 Equilibrium positions for a screw dislocation dipole with applied stress in the film for the three interface case. A minimum normalized applied stress of 1.8 is needed to keep the dislocations apart.

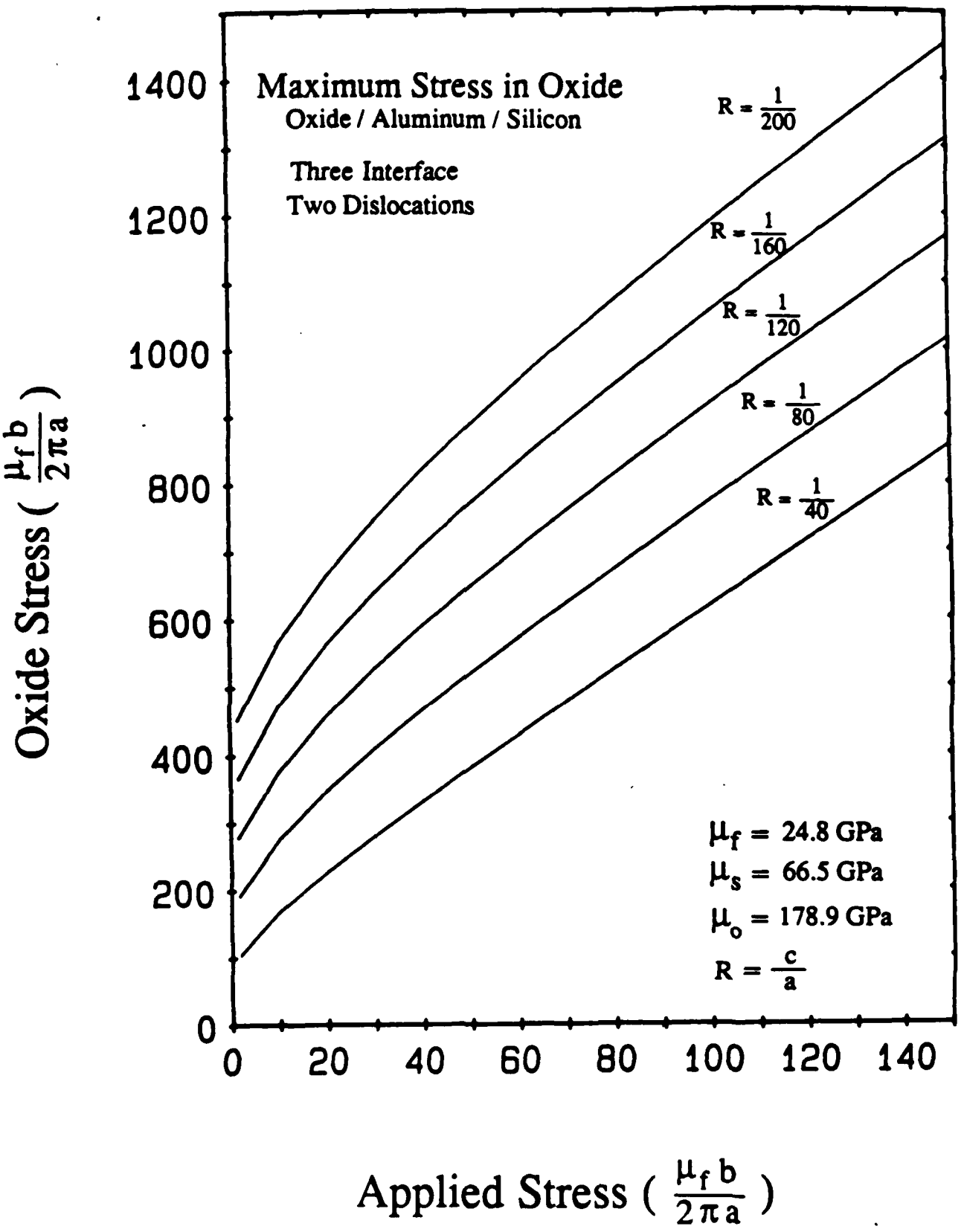

Fig. D5 Film-oxide stress as a function of the applied stress in the film for a screw dislocation dipole in the $Si/Al/Al_2O_3$ three interface case.

the interface. Likewise, the stress in the oxide is seen to increase with decreasing oxide thickness since the equilibrium position of the dislocation is closer to the interface for small R values.

The results given in this section of the report provide a theoretical foundation for the study of yielding in thin films. We expect to be able to predict the yield strengths of thin films by considering both the formation of dislocations at sources within the film and the subsequent movement of these dislocations toward the substrate and free surface. Such calculations will require the extension of the present results to multiple dislocations and the development of computer techniques of the kind used previously for the study of dislocation motion in two phase solids [1].

Reference

1. M.L. Ovecoglu, D.M. Barnett and W.D. Nix, accepted for publication in Acta Metallurgica

E. Study of Metal Cracking in Interconnect Metals
(A.I. Sauter and W.D. Nix)

Aluminum lines are commonly used as interconnects in integrated circuits. The metal is deposited and patterned into thin lines (typically about two microns wide) and then passivated with a glass. When the passivation glass is deposited at high temperatures, subsequent cooling causes hydrostatic tension stresses to develop in the lines due to the difference in thermal expansion between aluminum and its surroundings. These stresses cannot relax through plastic flow because the lines are bonded on all sides; consequently small cracks or cavities form to relieve the stresses. These metal cracks can lead to failure of the circuit. Although the phenomenon of metal cracking is quite well known and has been studied as an engineering problem, it has not been studied in a scientific way. Consequently we do not have a good understanding of the basic mechanisms of metal crack formation. To reach such an understanding it is necessary to develop techniques for studying the mechanisms and kinetics of metal crack formation and growth. We plan to use wafer curvature techniques to study the rate of cracking of metal lines as a function of temperature, stress, and passivation materials. Parallel metal lines will be deposited on a wafer and passivated. Using the wafer curvature technique to measure stress in the lines as a function of time, stress relaxation data may be obtained. These data can yield an activation energy for relaxation and can therefore provide information about the mechanism of crack formation. These kinds of measurements may indicate how the cracking can be minimized.

The first step in beginning to understand the metal crack problem is to estimate the stresses in the aluminum lines and the radii of curvature these stresses are likely to produce. Hence prior to making any measurements with the wafer curvature machine it is desirable to estimate the stresses in the lines for the test geometry under consideration. As a very rough first estimate, the stresses were assumed to be purely hydrostatic. Then we may write

$$\sigma = 3B\Delta\alpha\Delta T$$

where B is the bulk modulus of aluminum, $\Delta\alpha$ is the difference in thermal expansion

coefficients between aluminum and silicon, and ΔT is the maximum temperature change, taken to be 500 C in the present analysis. This gives an initial stress of 2,600 MPa, which yields a radius of curvature for the wafer of 1.90 m, through the relation,

$$\frac{1}{R} = \frac{6t_{Al}\sigma}{3E_{Si}(t_{Si})^2}$$

where

t_{Al} = thickness of the Al line = $2x10^{-4}$ cm
E_{Si} = 79,200 MPa
t_{Si} = thickness of the Si wafer = .05 cm.

The factor of 3 in the denominator is used because the aluminum is assumed to cover only one-third of the wafer. When the hydrostatic stress has relaxed to 0.9 of its initial value, the curvature becomes 2.11 m. These are clearly very high stresses and unrealistic curvatures. A more refined calculation is required.

Taking into account that the passivation is not infinite in extent but has some finite thickness, we model the passivation/line system by a cylinder of aluminum surrounded by a cylinder of SiO_2. Then using the misfitting thermal expansions as a boundary condition, and imposing a plane strain condition on the ends of the cylinder, the stresses in the aluminum lines were estimated to be an order of magnitude lower. Here, for a passivation thickness of 2μm, the same as the line width,

$$\sigma_{rr} = \sigma_{\theta\theta} = 370 \text{ MPa}$$
$$\sigma_{zz} = 260 \text{ MPa},$$

at maximum. This yields a minimum radius of curvature of 6.35 m, and a radius of curvature of 7.08 m when the stress has relaxed to 0.9 of its initial value. These are much more reasonable stresses and radii.

Using this model, the stresses are found to depend on the outer radius of the passivation cylinder, i.e. the thickness of the passivation, b, in μm, by the relation

$$\sigma_{rr} = \sigma_{\theta\theta} = \frac{528.7(b^2-1)}{b^2-0.274} \quad \text{MPa}$$

$$\sigma_{zz} = \nu\sigma_{rr} = 0.35\sigma_{rr}$$

Thus, for small b, the stresses can be quite small, going to zero for an outer radius of 1μm, which would correspond to no passivation as the aluminum was assumed to have a radius of 1μm. For large b, the stresses level off at 528.7 MPa and 370.1 MPa. These values are not as large as for the case ofhydrostatic stresses.

These estimates indicate that the curvature effects associated with stresses in passivated metal lines are in the measurable range and that it should be possible to study metal cracking by measuring changes of radius of curvature associated with time dependent crack formation and growth.

III. Oral Presentations Resulting from AFOSR Grant No. 86-0051

1. W.D. Nix, "Mechanical Properties of Microelectronic Thin Film Materials", CIS Annual Review, Stanford University, March 6, 1986.

2. W.D. Nix, "New Experimental Techniques for the Study of Mechanical Properties of Microelectronic Thin Films", Department of Mechanical Engineering, University of California, Davis, March 13, 1986.

3. W.D. Nix, "Mechanical Properties of Thin Films and Other Fine Scale Structures", Albuquerque Chapter of ASM, Albuquerque, New Mexico, March 19, 1986.

4. M.F. Doerner, "Mechanical Properties of Thin Films Using Nanoindenter Techniques", Materials Science Industrial Affiliates Program, Stanford University, May 28, 1986.

5. M.F. Doerner and W.D. Nix, "Mechanical Properties of Thin Films on Substrates", Micromechanics Research Group, IBM Research Laboratory, San Jose, California, June 27, 1986.

6. W.D. Nix and M.F. Doerner, "Mechanical Properties of Microelectronic Thin Film Materials: Nanoindenter and Wafer Curvature Techniques", Summer Research Group, Materials Science Center, Los Alamos National Laboratory, August 18, 1986

IV. Publications Resulting from AFOSR Grant No. 86-0051

1. M.F. Doerner and W.D. Nix, "A Method for Interpreting the Data from Depth-Sensing Indentation Instruments", J. Materials Research, 1, 601 (1986).

2. M.F. Doerner, D.S. Gardner and W.D. Nix, "Plastic Properties of Thin Fims on Substrates as Measured by Submicron Indentation Hardness and Substrate Curvature Techniques", J. Materials Research, 1, 845 (1986).

3. D.-B. Kao, J.P. McVittie, W.D. Nix and K.C. Saraswat, "Two-Dimensional Oxidation: Experiments and Theory", Proceedings of IEDM 85, IEEE, 1985, p. 388.

4. D.-B. Kao, J.P. McVittie, W.D. Nix and K.C. Saraswat, "Two-Dimensional Thermal Oxidation of Silicon: I. Experiments", (accepted for publication in IEEE Transactions on Electron Devices).

5. P.A. Flinn, D.S. Gardner and W.D. Nix, "Measurement and Interpretation of Stress in Aluminum Based Metallization as a Function of Thermal History" (accepted for publication in IEEE Transactions on Electron Devices).

6. M.L. Ovecoglu, M.F. Doerner and W.D. Nix, "Elastic Interactions of Screw Dislocations in Thin Films on Substrates", (submitted for publication in Acta Metallurgica).

7. D.-B. Kao, J.P. McVittie, W.D. Nix and K.C. Saraswat, "Two-Dimensional Thermal Oxidation of Silicon: II. Theory and Modeling", (submitted for publication in IEEE Transactions on Electron Devices).

END

5-81

DTIC